Angular distributions of deuterium desorption from modified Pd(111) surfaces - Experiments and simulation

Thesis

by
Johanna Stettner

for obtaining the academic degree
"Diplomingenieur"

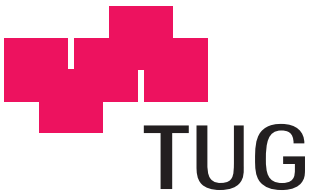

carried out at the
Institute of Solid State Physics
Graz University of Technology, Austria

under the supervision of
Ao. Univ.-Prof. Dipl.-Ing. Dr. techn. Adolf Winkler

Graz, Jänner 2007

Acknowledgement

This diploma thesis was performed under the supervision of Univ. Prof. Dr. tech. Adolf Winkler. I would like to thank for his brilliant mentoring and his dedicated and friendly support.

Dipl. Ing. Markus Kratzer introduced me into the experimental handling. I am grateful for his extraordinary helpfulness.

Moreover I would like to thank all members of the surface science group for the pleasant and cooperative working atmosphere.

Abstract

In this thesis, modified Pd(111) surfaces were investigated. The angular distributions of deuterium desorbing from clean Pd(111), Pd(111) + 0.3 MLE VO_x and Pd(111) + 0.2 ML K were measured at 523K and at 700K.
In general, one can assume the angular distribution of desorbing particles to have the form $cos^n\vartheta$. As the angular distribution was not measured by a directional detector but by lateral shift of the sample, Monte Carlo simulations were performed for different values of n. The measured angular distributions were assigned to simulated distributions in order to determine the values of n. For clean Pd(111), we obtained angular distributions of the form $cos\vartheta$ and $cos^2\vartheta$ at 523K and at 700K, respectively. The angular distributions of deuterium desorbing from Pd(111) + 0.3 MLE VO_x seem to be slightly sharper than from the clean Pd(111) surface. At Pd(111) + 0.2 ML K at 523K, the angular distribution of desorbing deuterium has the form $cos^3\vartheta$, which could be explained by a higher activation barrier for desorption. This result is in good agreement with earlier performed experiments.

In der vorliegenden Arbeit wurden modifizierte Pd(111) Oberflächen untersucht. Die Winkelverteilung von desorbierendem Deuterium wurde für reines Pd(111), Pd(111) + 0.3 MLE VO_x und Pd(111) + 0.2 ML K bei Temperaturen von 523K und 700K gemessen.
Im Allgemeinen nimmt man an, dass die Winkelverteilung desorbierender Teilchen von der Form $cos^n\vartheta$ ist. Da die Winkelverteilungen nicht mit einem Richtungsdetektor gemessen wurden, sondern durch laterale Verschiebung der Probe vor dem Detektor, wurden Monte Carlo Simulationen für verschieden Werte von n durchgeführt. Die gemessenen Winkelverteilungen wurden den simulierten Verteilungen zugeordnet, wodurch der jeweilige Wert von n bestimmt werden konnte. Für reines Pd(111) wurden Winkelverteilungen in der Form $cos\vartheta$ bei 523K und $cos^2\vartheta$ bei 700K erhalten. Die Winkelverteilungen für Pd(111) + 0.3 MLE VO_x scheinen unwesentlich schärfer als für reines Pd(111) zu sein. Die Winkelverteilung für Pd(111) + 0.2 ML K hat die Form $cos^3\vartheta$, was durch eine höhere Aktivierungsbarriere für Desorption erklärt werden kann. Dieses Resultat stimmt gut mit früher durchgeführten Experimenten überein.

Contents

1 Introduction **11**

2 Theoretical background **13**
2.1 Interaction processes of impinging particles on a surface 13
2.2 Adsorption 14
2.3 The sticking coefficient 16
2.4 The adsorption of hydrogen on metal surfaces 21
2.5 The concept of detailed balance 22
2.6 The angular distribution of desorbing particles 23
2.7 Some data about Palladium and Vanadium 24

3 Experimental Setup **25**
3.1 The vacuum equipment 25
3.2 The sample holder and the permeation source 26
3.3 The measurement equipment 27
3.4 The detector chamber 31

4 Measurement procedure **33**
4.1 Description of the angular distribution measurements 33
4.2 The evaporation process 36
4.3 Description of the permeation measurements 38

5 Simulation program for angular desorption distributions **43**
5.1 The analytical approach 43
5.2 Monte Carlo simulations 45
5.2.1 Design of the simulation program 46
5.2.2 Testing the program 51
5.2.3 Simulation results 57

6 Comparison of simulation results and measurements **59**
6.1 Comparison of measured angular distributions with simulation results . . 59
6.2 Comparison of the measured sticking coefficient with the angular distributions 64

7 Water formation on clean Pd(111) and on Pd(111) + 0.3 MLE VO_x: Measurement results **71**
7.1 Permeation measurements on Pd(111) and Pd(111) + 0.3 MLE VO_x 71
7.2 Comparison and discussion of the different permeation measurements . . . 72

8 Conclusion and Summary **75**

Appendix **77**

A Calculation of the desorption flux using the fit function S(E) **77**

B The simulation program code **81**

Bibliography **99**

Abstract

In this thesis, modified Pd(111) surfaces were investigated. The angular distributions of deuterium desorbing from clean Pd(111), Pd(111) + 0.3 MLE VO_x and Pd(111) + 0.2 ML K were measured at 523K and at 700K.
In general, one can assume the angular distribution of desorbing particles to have the form $cos^n\vartheta$. As the angular distribution was not measured by a directional detector but by lateral shift of the sample, Monte Carlo simulations were performed for different values of n. The measured angular distributions were assigned to simulated distributions in order to determine the values of n. For clean Pd(111), we obtained angular distributions of the form $cos\vartheta$ and $cos^2\vartheta$ at 523K and at 700K, respectively. The angular distributions of deuterium desorbing from Pd(111) + 0.3 MLE VO_x seem to be slightly sharper than from the clean Pd(111) surface. At Pd(111) + 0.2 ML K at 523K, the angular distribution of desorbing deuterium has the form $cos^3\vartheta$, which could be explained by a higher activation barrier for desorption. This result is in good agreement with earlier performed experiments.

In der vorliegenden Arbeit wurden modifizierte Pd(111) Oberflächen untersucht. Die Winkelverteilung von desorbierendem Deuterium wurde für reines Pd(111), Pd(111) + 0.3 MLE VO_x und Pd(111) + 0.2 ML K bei Temperaturen von 523K und 700K gemessen.
Im Allgemeinen nimmt man an, dass die Winkelverteilung desorbierender Teilchen von der Form $cos^n\vartheta$ ist. Da die Winkelverteilungen nicht mit einem Richtungsdetektor gemessen wurden, sondern durch laterale Verschiebung der Probe vor dem Detektor, wurden Monte Carlo Simulationen für verschieden Werte von n durchgeführt. Die gemessenen Winkelverteilungen wurden den simulierten Verteilungen zugeordnet, wodurch der jeweilige Wert von n bestimmt werden konnte. Für reines Pd(111) wurden Winkelverteilungen in der Form $cos\vartheta$ bei 523K und $cos^2\vartheta$ bei 700K erhalten. Die Winkelverteilungen für Pd(111) + 0.3 MLE VO_x scheinen unwesentlich schärfer als für reines Pd(111) zu sein. Die Winkelverteilung für Pd(111) + 0.2 ML K hat die Form $cos^3\vartheta$, was durch eine höhere Aktivierungsbarriere für Desorption erklärt werden kann. Dieses Resultat stimmt gut mit früher durchgeführten Experimenten überein.

Chapter 1

Introduction

The main task of surface science is the investigation of interactions between atoms or molecules with a solid surface. This includes to study the effect of special surface layers and structures on measurable quantities of interest, which is closely correlated with the growing field of nanoscience. E.g. the catalytic effect of surfaces can strongly depend on the special chemical composition and on the structure of the surface. Examinations of surfaces require ultra high vacuum conditions, as the surface has to stay clean to exclude an influence of undesired reactants. To investigate the surface of the sample, a sophisticated measurement equipment is required.

This thesis deals with desorption kinetics and dynamics on the Pd(111) surface. Palladium is an element of fundamental importance in industry. It is one of the best catalysts to produce water. It has the ability to absorb the maximum amount of hydrogen in the bulk, therefore it is used as hydrogen storage and for fuel cells. An important requirement for reproducible measurements is a proper palladium single crystal with known structure. In this thesis, we investigate the system Pd + 0.3 MLE VO_x. A surface film can have a promoting or a retarding effect on a reaction. The effect of vanadiumoxide covered palladium surfaces on the water reaction has not been known so far. It is an obvious task to study the system palladium with vanadiumoxide. Vanadium has several well known oxidation states on palladium. The vanadiumoxide nanostructures on the palladium surface can be quite different from the structure of vanadium oxide bulk. The present investigations are interesting in view of nanoscience as well.

We investigated a monocrystalline sample of Pd(111). Two different experiments were performed. The catalytic effect of palladium to generate water was investigated and the angular distribution of deuterium atoms desorbing from the palladium surface was measured. These measurements can be used to study desorption dynamics and kinetics. Let us clarify the distinction: To investigate dynamics, we consider the temporal development of a system. The path of individual reactions is examined. To investigate kinetics, averages of the entire surface physical processes are taken. It is not necessary to know the individual paths of a gas particle.

Investigations of the catalytic effect of palladium include measurements of reaction rates and desorption flux, which correspond to kinetics. Angular distribution measurements in turn can be used to investigate dynamics, since only particles moving in one specified direction are considered.

In general, one uses directional detectors to measure angular distributions. There are several opportunities to measure the angular distribution of desorbing particles when no directional detector is available. The angular distribution can be measured by shifting or tilting the sample holder. To quantify these measured angular distributions, one needs calculated angular distributions to compare the measured data with. One assumes the angular distribution to have the form $cos^n\vartheta$, which is an often approved approach. Angular distributions can be calculated according to this distribution for different values of n and for the same geometric situation as in the experiment. Comparison of the measured angular distribution with the calculated angular distribution gives a value for the exponent n.
We measured the angular distribution of deuterium desorbing from the palladium surface by shifting the sample parallel to the detector. To quantify the sharpness of the measured angular distribution, Monte Carlo simulations were performed. The used computer program can simulate the detected angular distribution for tilted and shifted samples in dependance of geometric parameters. Performing the simulation for the respective geometric parameters, we were able to compare the measured angular distributions with the simulation results to obtain the value of n.

If the principle of detailed balance is assumed to be valid, the sharpness of the angular distribution of desorbing particles is closely related to the energy dependance of the sticking coefficient of these particles, which is a quantity of general physical interest. As the sticking coefficient of deuterium on Pd(111) has already been measured by [1], we were able to compare our results with the angular distribution calculated by the energy dependance of the sticking coefficient of deuterium.

Chapter 2

Theoretical background

In this chapter, we will explain the theoretical background of the performed measurements: the physics of adsorption and desorption, the sticking-coefficient, the concept of detailed balance and normal energy scaling. The sample in use is a palladium crystal, which we can cover with vanadium. We will specify several properties of palladium and vanadium to motivate the use of these elements.

2.1 Interaction processes of impinging particles on a surface

When a molecule or an atom impinges on a surface, several possible reactions may occur (see [2]):

- Elastic scattering:
  As no energy exchange occurs, the particle is reflected back without any possibility to stick. The energy of the particle and the surface is conserved.
- Inelastic scattering:
  An energy transfer between particle and surface occurs - the particle may turn energy into the surface or receive energy from the surface. Anyway, the energy-loss of the particle is too low as to stick on the surface.
- Trapping:
  In this case, the molecule has lost enough of its energy to be trapped by the surface for some time, but a small energy transfer to the particle can cause it to leave the surface again.
- Adsorption:
  When the energy loss is high enough, the particle is bonded. The difference between trapping and adsorption is the time which the particle stays on the surface, which is much longer in case of sticking.

2.2 Adsorption

Adsorption is the adhesion of particles on a surface, unlike absorption, what means to imbibe the particles into the bulk.

To describe the adsorption process of a molecule quantitatively, the PES (potential energy surface, see [3]) of the molecule has to be considered. To describe the interaction of a diatomic molecule with a well defined surface, one needs at least a six - dimensional PES:
The parameters are the coordinates of the molecule, the azimuthal and polar orientation of the molecule and the bond distance between the two atoms. The calculation of a six - dimensional PES is in general quite complicated. Usually one can make simplifications without causing big errors.

The Lennard - Jones potential

To describe the adsorption of a two atomic molecule, e.g. hydrogen, on a metal surface, the two - dimensional Lennard - Jones potential is a good approximation (see [4]). The rotational and vibrational states are neglected, the potential energy of the system molecule - metal surface is considered in dependance of the reaction coordinate.

The path of a molecule AB approaching to a metal surface is considered ([5]). Only two forces acting on the hydrogen are taken into account: The attractive Van der Waals force and the Pauli repulsion.
The *Van der Waals force* is a rather weak attractive force caused by dipole interactions. It is often assumed to be of the form $\sim r^{-6}$.
The *Pauli repulsion* is attributed to the Pauli exclusion principle. It occurs when the wave functions of the molecule and the surface atoms are not separated anymore. Once the wave functions start to overlap, two electrons are not allowed to be in the same state according to the Pauli exclusion principle. Therefore, some electrons occupy higher states. This effects the Pauli repulsion, which is of the form $\sim r^{-12}$.

We consider the advancing process of a molecule AB and a molecule which is dissociated in its two atoms A+B, (see fig. 2.1). In general, the molecule or atom has to loose its kinetic energy to get trapped on the surface.

- The molecule AB first experience the weak attractive van der Waals potential. Near the surface, the repulsive potential due to the Pauli exclusion increases, so the molecule is repulsed. A molecule staying in this first potential minimum is called *physisorbed*. It is bonded to the surface only by Van-der-Waals forces and without chemical bonding by changing the electronic structure. This state is called a precursor-state, as the molecule is not fully bonded yet. In case of physisorbed adsorption, the molecule can only remain on the surface if it transfers its energy to the substrate.

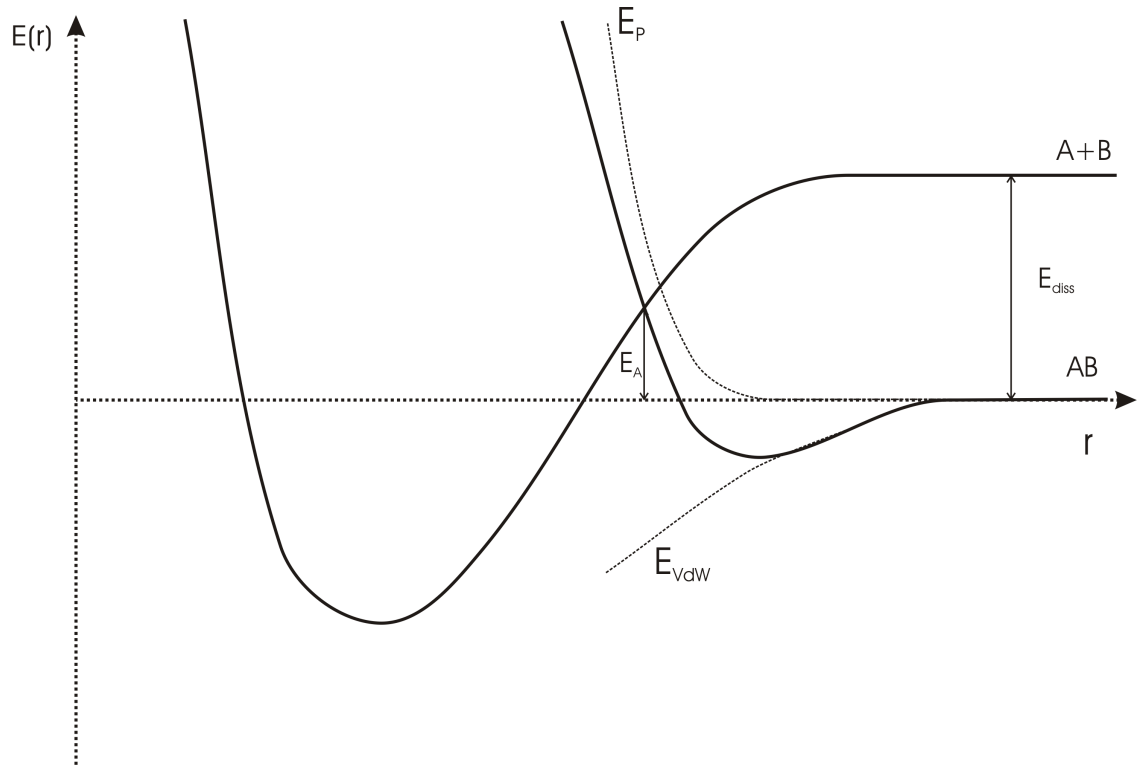

Figure 2.1: The potential curve for the Lennard-Jones-model. E_{VdW}: Van der Waals attraction, E_P: Pauli repulsion, E_A: Activation barrier, E_{diss}: Dissociation energy. The potential curve of dissociated elements A+B and the potential curve of an element AB intersect.

– The potential function for two dissociated atoms A+B, for example two hydrogen atoms, behaves differently: The potential far from the surface is much higher than in case of a molecule, as some energy is spent to dissociate. With decreasing distance to the surface, they fall into a large potential minimum. Atoms bonded in this state are *chemisorbed*. So the kinetic energy of the molecule can be transferred into the bond breaking. The probability for dissociative adsorption is almost entirely given by the dissociation probability.

The potential curve for a molecule and the potential curve for dissociate atoms intersect, so a physisorbed molecule has the opportunity to dissociate and to adsorb by chemisorption. Depending on whether the cross point lies at positive or negative energies, an activation barrier exhibits or not. The chemisorption is much stronger than the physisorption, since the charge of the atoms is changed. The atoms are bonded chemically to the surface.
It is also possible for a dissociated molecule to straightly adsorb without before being bonded in a precursor state.

Of course, the adsorption process depends on many parameters as the temperature, the surface coverage, the energy of the incident particles and the angle of the incident particles.

A quite useful value for describing adsorption processes is the sticking coefficient, which will be explained in the next section.

2.3 The sticking coefficient

The sticking coefficient is the probability of particles to adsorb on a surface:
It is defined by the ratio of the number of adsorbing particles N_{ads} and the number of impinging particles N_{imp}:

$$S = \frac{N_{ads}}{N_{imp}} \tag{2.1}$$

Experimentally, the sticking coefficient is determined by measuring the amount of adsorbed and impinged particles.
The impingement rate Z is correlated with the gas pressure p by

$$Z = \frac{p}{(2\pi mkT)^{\frac{1}{2}}}. \tag{2.2}$$

The sticking coefficient is a function of different parameters, as the electronic structure of the surface, surface defects, the coverage and the surface temperature (see [6]).
These parameters can have different effects on the sticking coefficient depending on the bond between the molecule and the surface. One has to distinguish between **physisorbed particles** and **chemisorbed particles**.
In case of chemisorbed particles, there is a difference between *straight chemisorption* and *chemisorption through a precursor path.*

In general, two points are essential for a particle to be able to stick: The energy of the particle has to be high enough to overcome a possible activation barrier. In addition, the normal component of the translational energy of the incident particle has to vanish.
Now we will consider several dependencies of the sticking coefficient:

- **temperature dependance of the sticking coefficient**

  Straight adsorption without precursor is in general not surface temperature dependent. Therefore a temperature dependent sticking coefficient is a hint for a precursor mediated adsorption. When the molecule is bonded in a precursor state, its transition probabilities into the chemisorbed state or for desorption are temperature dependent.

  If an activation barrier exists in the chemisorbed state, the sticking coefficient increases with temperature because the activation barrier can more easily be transgressed at higher temperatures. In case of precursor assisted, non-activated adsorption, the sticking coefficient decreases with temperature.

– **coverage dependance of the sticking coefficient**

The sticking coefficient on a clean surface without already adsorbed particles is called the initial sticking coefficient. When the number of particles on the sample surface increases, the sticking coefficient usually decreases. At a saturation coverage N_{sat} the sticking coefficient approaches to zero.
A simple approach to calculate the coverage dependance of the sticking coefficient has been given by Langmuir. He supposed an incident particle to stick on an empty adsorption place with a certain probability S_0, and to be scattered on an occupied adsorption place with probability one. In other terms: all adsorption sites are equivalent and the adsorption is limited by the monolayer coverage.
Thus one gets for the adsorption rate r_{ads}, when Θ is the coverage, the so called Langmuir adsorption law:

$$r_{ads} = S(\Theta) \cdot Z = S(0) \cdot (1 - \Theta)^n \cdot Z. \tag{2.3}$$

n is the number of places that are needed to adsorb the molecule or particle.

This law is a good approximation, but it does not describe the reality in many cases, as for example adsorption through a precursor state is not considered.

– **energy dependance of the sticking coefficient:**

When considering the energy dependance of the sticking coefficient, it is important to keep in mind the concept of *normal energy scaling*: In many cases, one can assume the adsorption process to depend merely on the normal component of the translational energy. This behavior is called 'normal energy scaling' (NES) and simplifies many calculations. If the surface is structureless and flat, the parallel momentum of the incident particle is conserved. This implicates a sticking coefficient which depends only on the normal component of the translational energy:

$$E_\perp = E \cdot cos^2\vartheta. \tag{2.4}$$

The cos^2 - dependence can be explained by the following consideration:

$$E = \frac{mv^2}{2} = \frac{m(v_\perp + v_\parallel)^2}{2}. \tag{2.5}$$

Since

$$v_\perp = v \cdot cos\vartheta$$

one gets:

$$E_{\perp} \sim cos^2\vartheta. \tag{2.6}$$

To adsorb on a surface, a particle has to loose its normal translational energy.

In case of direct, non-activated adsorption, the sticking coefficient usually is independent on the energy. At very high energies, the sticking coefficient may decrease in this case, since the particle can not loose its energy, because the potential wall is to low.

In contrary, when an activation barrier exists, the sticking coefficient increases with translational energy. The probability to overcome the activation barrier grows with increasing energy.

There are precursor mediated systems for which an alternative activated adsorption path exists. At low translational energy, the adsorption is precursor mediated while at high translational energies, activated adsorption occur.

– **angular dependance of the sticking coefficient**

The sticking coefficient is expected to change with the angle of incidence of the adsorbing particles. The angular dependance of the sticking coefficient is closely related to its energy dependance.

Assuming NES to be valid, one finds for the sticking coefficient:

$$S(E, \vartheta) = S(Ecos^2\vartheta, 0°). \tag{2.7}$$

So the slope of the function $S(E)$ is related to the sharpness of the function $S(\vartheta)$.

By the following considerations one can find an expression for the angular dependance of the sticking coefficient:

The sticking coefficient can be defined as ratio of adsorption rate $A(\vartheta)$ to impingement rate $Z(\vartheta)$. By geometrical considerations one can easily find that:

$$Z(\vartheta) = Z_0 \cdot cos\vartheta. \tag{2.8}$$

The adsorption rate $A(\vartheta)$ can be described by the following angular dependance:

$$A(\vartheta) = A_0 \cdot cos^n\vartheta. \tag{2.9}$$

Thus one gets for $S(\vartheta) = \frac{A(\vartheta)}{Z(\vartheta)}$:

$$S(\vartheta) = S_0 \cdot cos^{n-1}\vartheta. \tag{2.10}$$

Furthermore,

$$A(\vartheta) = S(\vartheta) \cdot cos\vartheta. \tag{2.11}$$

The knowledge of this exponent n is quite useful, as it delivers information about the energy dependance of the sticking coefficient and about the angular distribution of the adsorption rate.
The energy dependance of S can be written as:

$$S(E) = S_0 \cdot E^{\frac{n-1}{2}}. \tag{2.12}$$

Let us consider the formulas (2.9), (2.11) and (2.12) for different values of n:

$n = 1$**:**
The sticking coefficient is independent on the energy and therefore independent on the angle as well. This is related to a cosine dependance of the adsorption rate $A(\vartheta)$. Physically, this situation describes a direct, non-activated adsorption.

$n > 1$**:**
In this case, the sticking coefficient increases with energy. The angular distribution of the adsorption rate $A(\vartheta)$ is sharper than cosine. This corresponds to activated adsorption.

$n < 1$**:**
As the sticking coefficient decreases with energy (and with angle ϑ), one gets a broad angular distribution for the adsorption rate $A(\vartheta)$. This situation describes a precursor mediated adsorption.

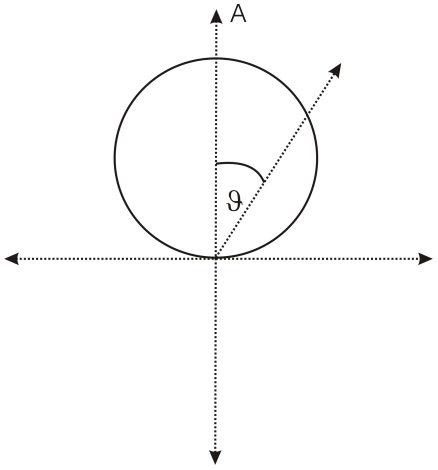

(a) The adsorption rate $A(\vartheta)$ has the form of $cos\vartheta$

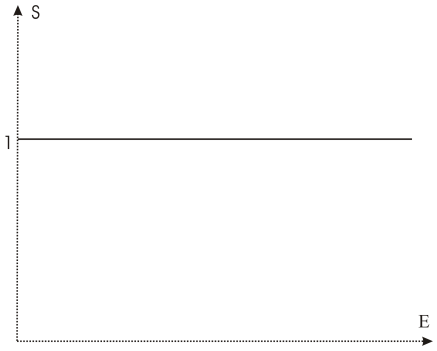

(b) The sticking coefficient $S(E)$ is constant

Figure 2.2: The adsorption rate and the sticking coefficient of a gas when assuming it to adsorb according to the $cos^n\vartheta$ - distribution with $n = 1$

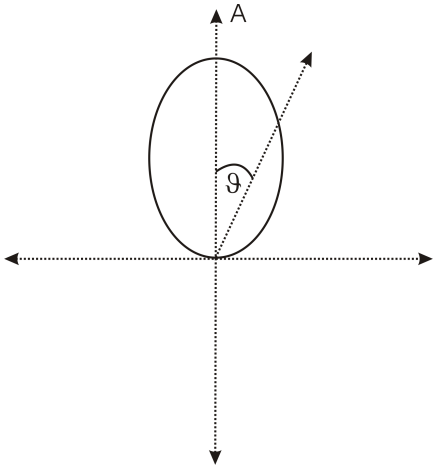

(a) The adsorption rate $A(\vartheta)$ is sharper than $cos\vartheta$

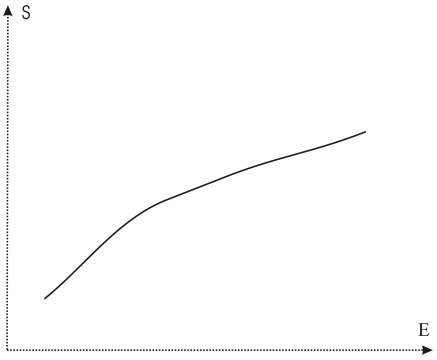

(b) The sticking coefficient $S(E)$ increases

Figure 2.3: The adsorption rate and the sticking coefficient of a gas when assuming it to adsorb according the $cos^n\vartheta$ - distribution with $n > 1$

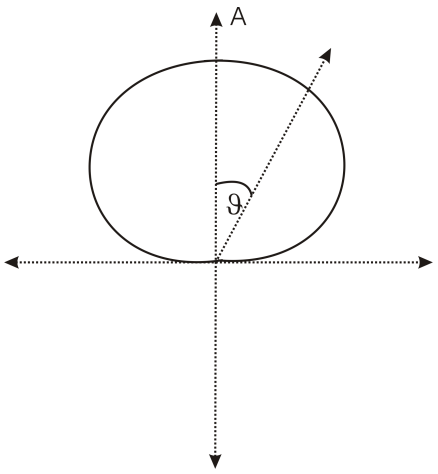

(a) The adsorption rate $A(\vartheta)$ is broader than $cos\vartheta$

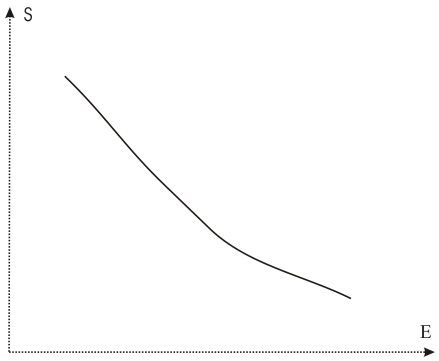

(b) The sticking coefficient $S(E)$ decreases

Figure 2.4: The adsorption rate and the sticking coefficient of a gas when assuming it to adsorb according the $cos^n\vartheta$ - distribution with $n < 1$

2.4 The adsorption of hydrogen on metal surfaces

When considering the adsorption of hydrogen on metals one often finds a steep negative slope for the sticking coefficient at low energies. A scheme of the sticking coefficient for such systems is shown in fig. 2.5. The decrease of the sticking coefficient is usually described by a precursor state. There exists an alternative explanation for this behavior, when the rotation of the molecule is considered: The **steering effect**.

The adsorption of a molecule can be hindered or enhanced depending on the orientation of the rotational axis of the molecule. If the rotational axis of the molecule is parallel to the surface (cartwheel rotation), the adsorption is hindered. In contrast, helicopter rotation, which means that the rotational axis of the molecule is normal to the surface, advantages the adsorption process (see fig. 2.6).

At low kinetic energies, a molecule can turn in an advantageous position to adsorb on the surface. So most slowly rotating impinging molecules steer towards the attractive dissociation channel which leads to a high adsorption probability (see [7]). As energy is converted into internal degrees of freedom, this energy is not available for a direct escape from the surface.

The steering effect is suppressed for higher energies. If the molecule rotates quickly, it rather gets out of the advantageous position. So the high sticking probability at low energies is caused not only by trapping into a physisorption state, but mainly by steering effects.

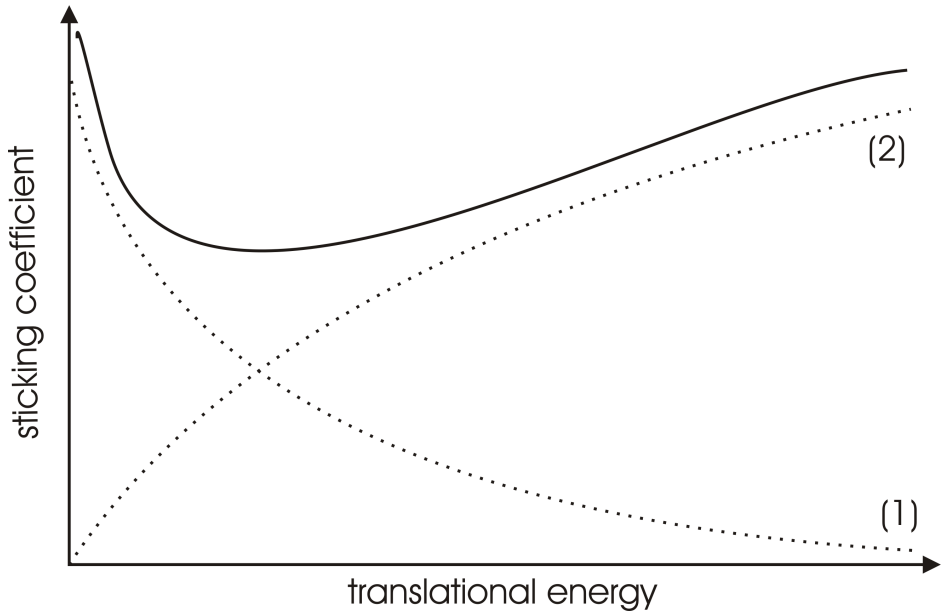

Figure 2.5: The sticking coefficient for a system with a precursor path (1) and a direct activated path (2)

2.5 The concept of detailed balance

As Langmuir put it in 1916 (see [8]):
'Since evaporation and condensation are in general thermodynamically reversible phenomena, the mechanism of evaporation must be the exact reverse of that of condensation, even down to the smallest detail.'

Let us perform a thought experiment:

A closed room with particles inside in chemical equilibrium is observed. Being in thermal equilibrium, the adsorption probability of a particle is equal to the desorption probability. Each particle adsorbing on a surface under an angle ϑ corresponds to another particle desorbing under the angle ϑ.

When a system is in thermal equilibrium, one can formulate the following principle (see [9]):

$$S(\theta) \cdot cos\vartheta = A(\vartheta) = D(\theta) \tag{2.13}$$

Here, $D(\vartheta)$ is the desorption probability. It can be shown that this equation is valid even under quasi-equilibrium conditions.

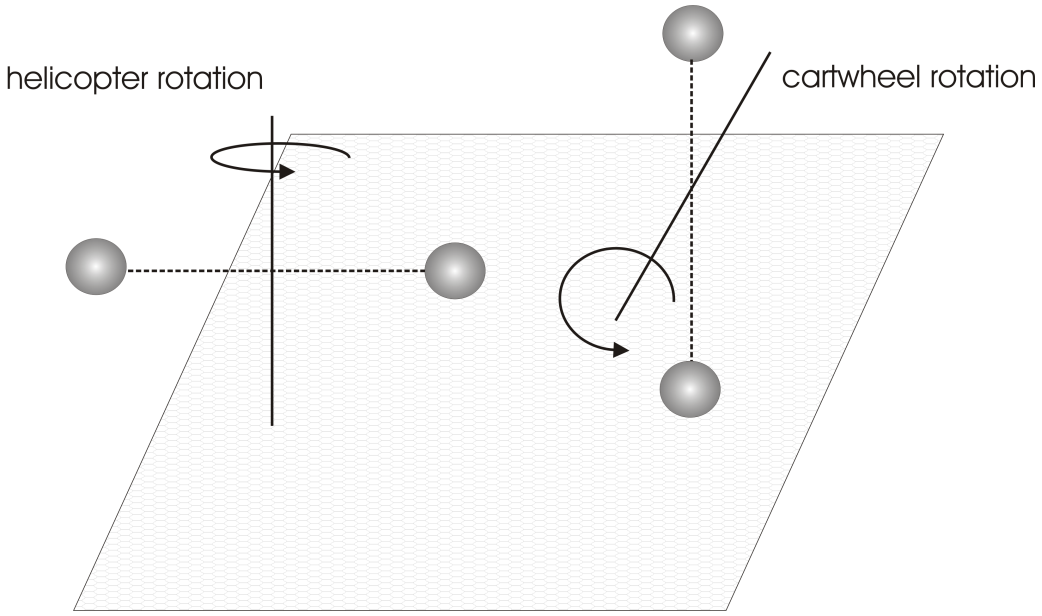

Figure 2.6: If the rotational axis of the molecule is parallel to the surface (cartwheel rotation), the adsorption is hindered. Helicopter rotation, which means that the rotational axis of the molecule is normal to the surface, advantages the adsorption process.

(2.13) should still be valid even if the system is not in thermal equilibrium. Examinations have been done by measurements: Although it is not possible to measure under ideal conditions, (2.13) has been proved to be sufficiently exact.
So it is possible to get the angular dependance of the sticking coefficient by the angular dependance of the desorbing particles.

2.6 The angular distribution of desorbing particles

Some times ago, one believed that particles desorbing from a surface obey the cosine distribution. Later, one recognized that only the sum of all particles leaving a surface has to be a cosine. This includes not only desorbing particles but also elastically and inelastically scattered particles. Van Willigen [10] showed in a famous experiment that hydrogen desorbing from metal surfaces exhibits strongly forward focussed angular distributions. This can easily be explained:
To pass over the activation barrier, the normal component of the translational energy $E \cdot cos^2\vartheta$ has to be larger than the activation energy E_A. With increasing angles fewer and fewer particles are able to transgress the barrier. An approach to describe the angular dependence of the desorption rate is given by:

$$D(\vartheta) = D_0 \cdot cos^n\vartheta \tag{2.14}$$

Most of experimental results concerning angular distributions can be described by this dependance (see [11],[12]). Following the principle of detailed balance, the same dependence is assumed to be valid for the adsorption rate. By the use of $S(E, \vartheta) = S(Ecos^2\vartheta, 0°)$, one gets furthermore (see [13])

$$S(E) = S_0 \cdot E^{\frac{n-1}{2}}. \tag{2.15}$$

2.7 Some data about Palladium and Vanadium

– **Palladium**

The sample in use is a palladium single crystal. Palladium is a transition metal of the platinum group with atomic number 46. It is the most reactive element of the platinum group. Its melting point is 1828 K, its boiling point 3236 K (see[14]). At room temperature, it does not react with oxygen, so it does not tarnish in air.
It is the element with the ability to absorb the maximum amount of hydrogen. At room temperatures, it is able to absorb several hundred times its own volume of hydrogen. Moreover, it is a very good catalyst for water generation, wherefore it is mainly used in industry. At high temperatures, hydrogen diffuses quickly through thin palladium pieces, so it can be used as permeation source. In this case, palladium has a purifying effect as well. Palladium can be used as hydrogen storage and for fuel cells.

– **Vanadium**

The palladium sample was evaporated with vanadium. Vanadium is a transition metal with atomic number 23. It has a melting point of 2175 K and a boiling point of 3680 K (see[14]). Vanadium is mostly used as component in steel to improve the properties of the steel.
Vanadium reacts easily with oxygen: there are several oxidation states. On a palladium surface, thin vanadium layers form a variety of nanostructures.

Chapter 3

Experimental Setup

In this chapter, the experimental setup of the UHV (ultrahigh vacuum) chamber is described. The UHV system is explained and the use of a permeation source and a special detector chamber is motivated. In addition, the measurement equipment and the theoretical background of the analyzing methods are described.

3.1 The vacuum equipment

Our experiments were performed in a UHV chamber. We need UHV conditions, as we investigate the surface of the palladium sample. It is important to keep the surface clean, which requires the pressure to be below 10^{-9} mbar.

The used vacuum system is divided into two chambers which are separately pumped. The measurement devices are installed in the main chamber. To measure the particles coming out of the sample surface, a special detector chamber is used. The main chamber and the detector chamber are joined by a bypass, which is closed during measurements.
The main chamber is separated in two parts by a gate-valve. The lower part contains a turbomolecular pump (LEYPOLD Turbovac 360, pumping speed $S = 345$ l/s) and a titanium sublimation pump. The upper part contains a turbomolecular pump with $S = 520$ l/s and a small turbomolecular pump (Pfeiffer TMU 071 P, $S = 60$ l/s). As forepump, a rotary vane pump (Pfeiffer DUO 20, $S = 20\ m^3/h$) is used.
In the detector chamber, a sputter ion pump with $S = 20\ l/s$ is installed.
Several additional actions have been taken to reach pressures in the range of $p = 1 \cdot 10^{-10}$ Torr. After pumping down the vacuum system, the chambers have been baked out. This is done for at least 24 h at temperatures in the range of 130°C. To reduce the pressure, the sample holder has been LN_2 - cooled during measurements.

An extractor ionization gauge (LEYBOLD Ionivac IM 510) is used to measure the pressure in the main chamber.

3.2 The sample holder and the permeation source

The sample holder is installed in the main chamber. The sample holder can be rotated by 360° and shifted nearly ±20 mm in all three directions of space.

For this thesis, two experiments were performed: we investigated the catalytic effect of palladium to produce water and we measured the angular distribution of deuterium particles desorbing from the palladium surface. In both experiments, a constant deuterium flux for at least half an hour is demanded.
This requirement can be fulfilled by using the palladium sample as a permeation source. Palladium is an appropriate material for a permeation source: It has the ability to absorb the maximum amount of hydrogen in the bulk.

The construction of the permeation source (see [15], [16]):

The palladium sample (10 mm in diameter, 1 mm thickness) is welded into a high purity nickel-cylinder. A stainless steel cap is welded onto the nickel cylinder. The cap contains a stainless steel pipe, which is used for gas inlet. The setup is covered with ceramics, in which a molybdenum heating coil is embedded. The molybdenum coil is used to heat the sample up to 1000K. A scheme of the permeation source is shown in fig. 3.1.
From the backside of the sample, the deuterium is applied at high pressures. The deuterium is forced to adsorb on the palladium and to diffuse through it. At the outer surface, the permeated deuterium desorbs at low pressure from the palladium surface. The cylindrical mounting has a much lower permeability for deuterium, so it is guaranteed that most of the deuterium absorbing in the palladium desorbs from the palladium surface on the outer surface. The pressure at the backside of the permeation source is measured by a piezo - membrane gauge. During measurements, this pressure is in the range of 1 mbar.
The permeation of deuterium (instead of adsorbing and desorbing it) has many advantages. The desorbing deuterium flux is almost constant for a time in the range of some hours. In addition, the palladium has the ability to clean the deuterium flux.

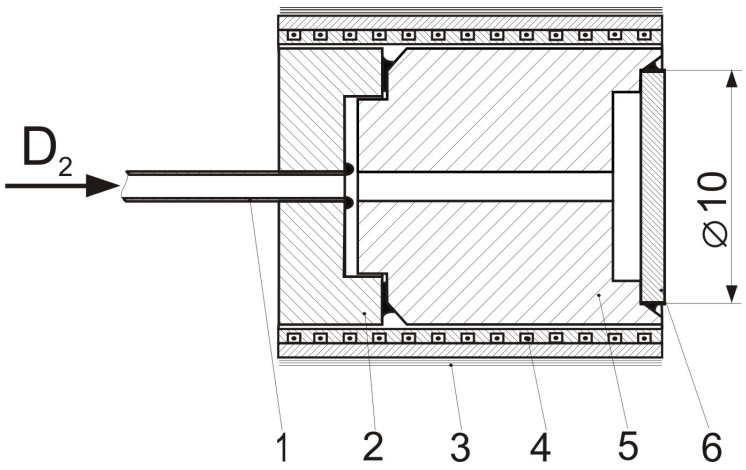

Figure 3.1: Cross-section of the permeation source. 1: stainless steel pipe, welded to the stainless steel cap, 2: stainless steel cap, 3: several layers of tantalum foil for radiation shielding, 4: molybdenum heating coil embedded in ceramics, 5: high purity Ni-cylinder, 6: palladium sample

3.3 The measurement equipment

Several measurement devices are installed in the main chamber to prepare and to analyze the sample surface.

1. LEED (low energy electron diffraction) is used to analyze the surface structure.
2. AES (Auger electron spectroscopy) is employed to determine the composition of the surface.
3. To measure the partial pressures, two QMS (quadrupole mass spectrometer) are installed: one in the main chamber, another in the detector chamber
4. The sample surface is cleaned via sputtering by an argon - gun.
5. An evaporator creates the vanadium - film
6. The respective pumping speed of the two chambers is determined by two tungsten coils

The measuring setup is shown in fig. 3.2
In addition, the theoretical background of the different analyzing methods will be explained (see [17]).

ad 1)

LEED is used to analyze the surface structure of a sample. The LEED optics consists

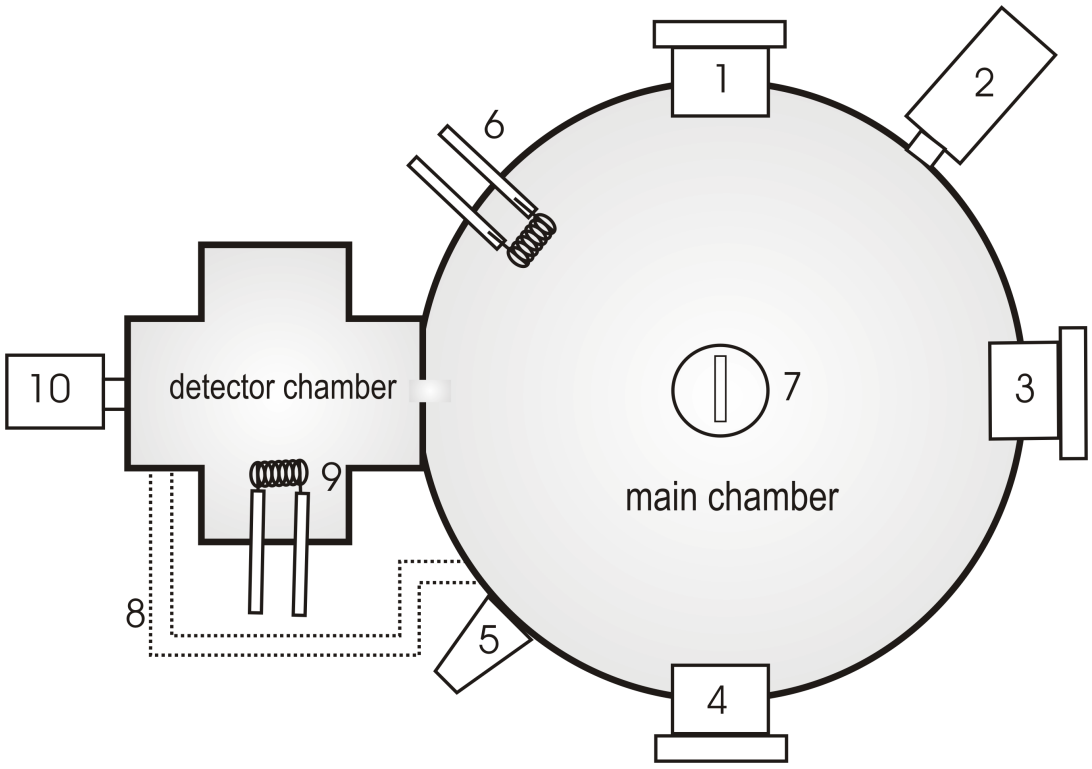

Figure 3.2: Scheme of the measuring setup:
1: LEED. 2: QMS. 3: AES. 4: Evaporator. 5: Argon-Gun. 6: Tungsten-coil. 7: Sample-holder. 8: Bypass. 9: Tungsten-coil. 10: QMS.

of an electron gun which emits electrons with energies in the range of 30-500 eV. These electrons reach the well ordered sample surface, where they are scattered. As they have a de Broglie wave length of some Angström, they interfere on the lattice of the solid surface. The scattered electrons arrive at a grid on which a negative voltage is impressed. This voltage is only some volt smaller than the acceleration voltage. Therefor only elastically scattered electrons, for which the energy is conserved, pass the grid. These are accelerated at a fluorescent screen, where they produce a light spot. The observed LEED pattern is the reciprocal lattice of the real surface lattice.

ad 2)

AES is used to analyze the chemical composition of the surface. The Auger-process forms the basis of this analyzing method: an excited atom emits an electron near the core level. Another electron refills the hole and the energy can be transferred to a third electron which leaves the atom. These so called Auger electrons have a characteristic energy in the range of 10eV - 2keV. This corresponds to a mean free path in the range of several atomic layers whereby AES becomes surface sensitive. The Auger electrons are analyzed by a cylindrical mirror analyzer, through which only electrons with a certain energy are able to pass.

ad 3)

A QMS serves to detect particles according to their mass. Generally, a mass spectrometer consists of an ion source, an analyzer and a detector.
The ionized particles are passing an analyzer, where they are separated according to their mass to charge ratio. In case of a quadrupole mass spectrometer, the analyzer consists of four parallel electrodes. Opposite electrodes have the same potential, and the electrodes side by side have a voltage of $U(t) = \pm U + V cos(\omega t)$. The particles are diverted by a rod system and subsequently detected by a secondary electron multiplier. For our measurements, the QMS serves as a partial pressure analyzer. To get the partial pressures of the individual components, the QMS has to be calibrated with a spinning rotator gauge. By this way, one gets a correction factor for each individual species of gas.

ad 4)

An ion sputter gun is used to clean the surface: argon - ions sputter the atoms, which are adsorbed on the palladium surface. This can lead to defects on the surface, which have to be healed at high temperatures. This so called annealing is done at 900K. Sometimes, annealing is done under oxygen-pressure, because the oxygen atoms recombine with the atoms on the surface and they together desorb (for example carbon becomes carbondioxide and leaves the surface). In general sputtering is done at high temperature, but there are some exceptions. Vanadium on the palladium surface should not be sputtered at high temperatures, as the vanadium tends to diffuse into the palladium bulk at high temperatures. For this system, it is important to sputter at temperatures not much higher than room temperature.

ad 5)

The vanadiumoxide layer on the palladium surface has been realized by electron beam evaporation. An oscillating quartz crystal is used to measure the deposit amount: It is possible to calculate the respective change of frequency Δf of the oscillating crystal for a certain evaporated layer thickness D. One evaporates vanadium on the oscillating crystal and checks the time $\Delta\tau$ until the desired frequency variation is reached. One evaporates vanadium on the sample surface for the same time. The integrale mass sensitivity of the oscillating crystal $S = 2.27 \cdot 10^{-6}\ s\ cm^2/g$ and the area density of 1 ML vanadium $n_{vanadium} = 1.2911 \cdot 10^{-7}$ g$/cm^2$ on palladium is known. One can calculate the necessary frequency variation for a certain vanadium coverage by:

$$\frac{\Delta f}{f} = -\frac{\Delta\tau}{\tau} = -\frac{\Delta n}{n} \tag{3.1}$$

As

$$\frac{\Delta\tau}{\Delta n} = S \tag{3.2}$$

it follows

$$\frac{\Delta f}{f} = -\frac{\rho\Delta D}{n} = -\frac{\rho \cdot \Delta D \cdot S}{\tau} = -f \cdot \rho \cdot \Delta D \cdot S \tag{3.3}$$

where $\rho \cdot D$ corresponds to an area density.

The oscillation frequency of our oscillating crystal is approximately 6 MHz. For our frequently used 0.3 ML vanadium coverage the needed frequency change is 3.5 Hz.
To obtain vanadiumoxide on the palladium surface, we evaporated the vanadium under oxygen atmosphere ($p_{O_2} = 1 \cdot 10^{-7}$ Torr). The amount of adsorbed vanadiumoxide is then designate as MLE (monolayer equivalent). When evaporating 0.3 ML vanadium under oxygen pressure, we call the obtained vanadiumoxide layer 0.3 MLE VO_x.

ad 6)

Two tungsten coils are used to get the pumping speed for hydrogen of the main chamber and of the detector chamber. The coil is calibrated when the saturation coverage is known. The hydrogen atoms on the coil desorb when the coil is heated. When considering the hydrogen pressure, one notice a steep increase of the pressure at the time of heating. The area under this peak is proportional to the amount N_{des} of particles causing the pressure increase. Thus one gets the pumping speed S by:

$$S = \frac{N_{des}}{K} \cdot \frac{1}{\int \Delta p(t)\, dt} \tag{3.4}$$

with K a constant $K = 3,27 \cdot 10^{19}$ molecules/(Torr·l)
The saturation coverage N_{des} of the tungsten filament used in our vacuum chamber has been determined to be (see [15])

$$N_{des} = 1.33 \cdot 10^{15}[\text{H-atoms}]. \tag{3.5}$$

3.4 The detector chamber

In the main chamber always exists a background signal: The main chamber is flooded with oxygen and deuterium during measurements and most measurement devices are installed herein. The noise caused by reactions on hot filaments or on the chamber walls is quite high. Therefore, the detector chamber is used to measure the particles desorbing from the palladium surface. In the detector chamber, a special line - of - sight mass spectrometer is installed, which improves the signal. If the sample surface is turned to the front of the detector chamber, only particles desorbing from the palladium surface are detected. The arrangement of the chamber is shown in fig. 3.3

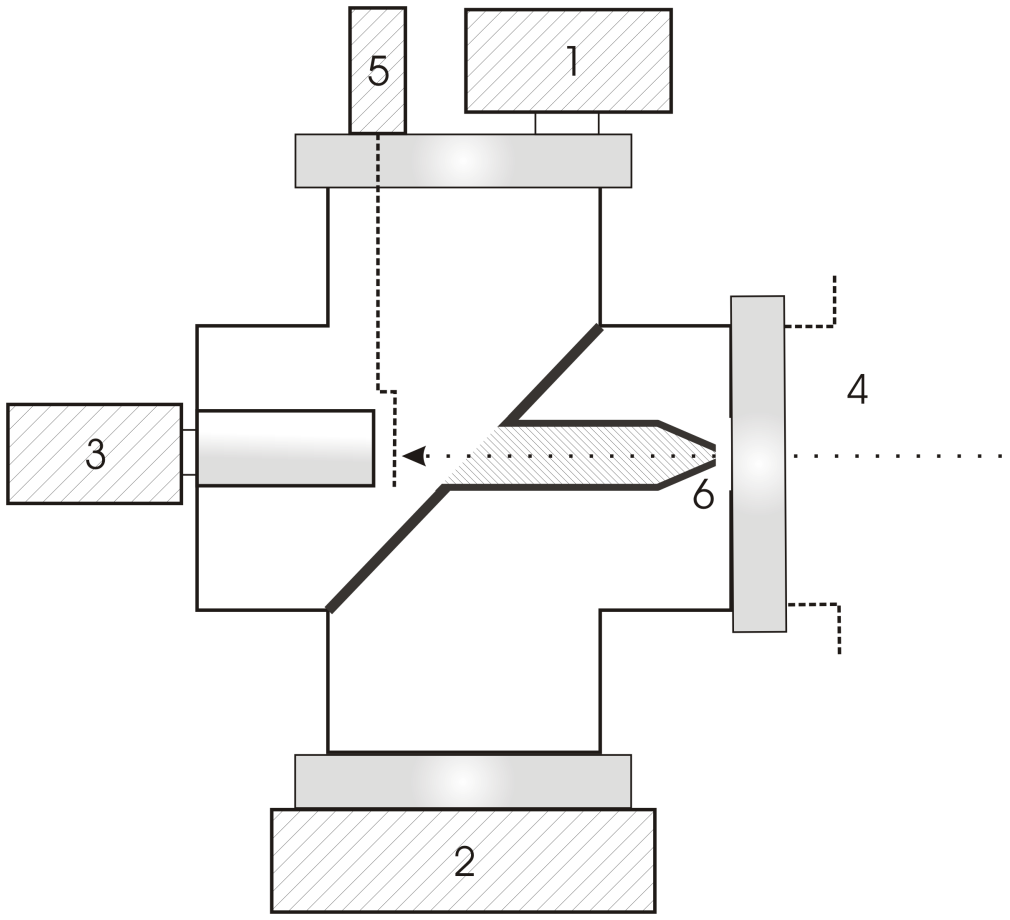

Figure 3.3: Scheme of the detector chamber:
1: Ion-pump with pumping speed $S = 20$ l/s; 2: Turbo-molecular-pump with pumping speed $S = 520$ l/s. This pump does not pump the detector chamber! It is connected to the main chamber; 3: QMS; 4: Main chamber; 5: The rotary feed through with shutter 6: Aperture

There are some other features in the detector-chamber: A shutter can be set in front of the line - of - sight detector. In this case, the particles do not fly directly into the detector.

This is important for flux measurements, since the detected particle density depends on the velocity of the measured particles. Only when the particles randomize before flying in the detector, one gets proper measurement signals.

Chapter 4

Measurement procedure

Two experiments were performed for this thesis: the catalytic effect of palladium to produce water was investigated and the angular distribution of deuterium atoms desorbing from the palladium surface was measured. In this chapter, the measurement procedure is described for these two types of measurements. The measurement difficulties are discussed and several raw data are shown.

4.1 Description of the angular distribution measurements

In the following section, the measurement procedure for the angular distribution of deuterium-particles desorbing from the Pd(111) surface is explained:
The base pressure of the used vacuum system is $1 \cdot 10^{-10}$ Torr. The sample is heated to a certain temperature (our experiments were performed at 523K and at 700K). The sample is turned to the front of the detector chamber. The deuterium valve is opened. After a while, an almost constant deuterium flux permeates through the surface, until the pressure in the chamber increases until approximately $p_{HK} = 8 \cdot 10^{-10}$ Torr. Afterwards, the oxygen valve is opened until the pressure in the main chamber is raised till approximately $p_{HK} = 5 \cdot 10^{-8}$ Torr. Then, the angular distribution is measured:
The sample is displaced parallel to the detector from the left to the right in x-direction as shown in fig. 4.1.

The shifted way has a length of 40 mm. To measure the angular distribution, the sample holder is moved at a time by 2 mm. The sample stands for 1 minute at each position. At the beginning and at the end of the measurement, the sample holder is turned 180° away. Thereby, the background signal can be determined. The background is subtracted in the later analysis.

One can see the measured raw data in fig. 4.2. Often, it is not possible to determine the exact location of the maximum. It seems that the 'zero-point', where the emitter is in front of the detector, is shifted by approximately 1 mm. This has to be considered when

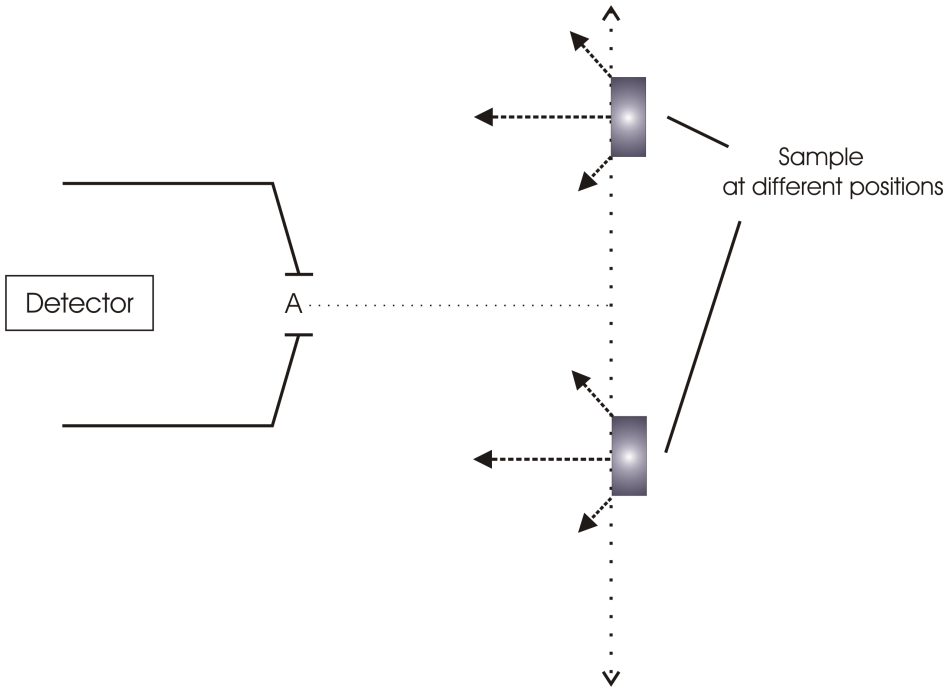

Figure 4.1: The angular distribution is detected by displacing the sample in front of the detector. A: aperture. Geometrical parameters: radius of the sample: $r_e = 3.5$ mm, radius of the aperture $r_d = 4$ mm, distance between sample and aperture: $d = 17$ mm.

analyzing the data, see chap. 6.

During the measurements, the bypass between main chamber and detector chamber was closed. The measurements were performed at two different temperatures and for three different sample preparations:

- Pd(111) clean at 523K and at 700K
- Pd(111) with 0.2 ML potassium at 500K
- Pd(111) with 0.3 MLE VO_x at 523K and at 700K

The angular distribution of deuterium desorbing from Pd(111) with 0.2 ML potassium is quite well known (see [18]). The measured angular distribution is compared with earlier performed measurements to prove the correctness of the measurement procedure and of the simulation results.

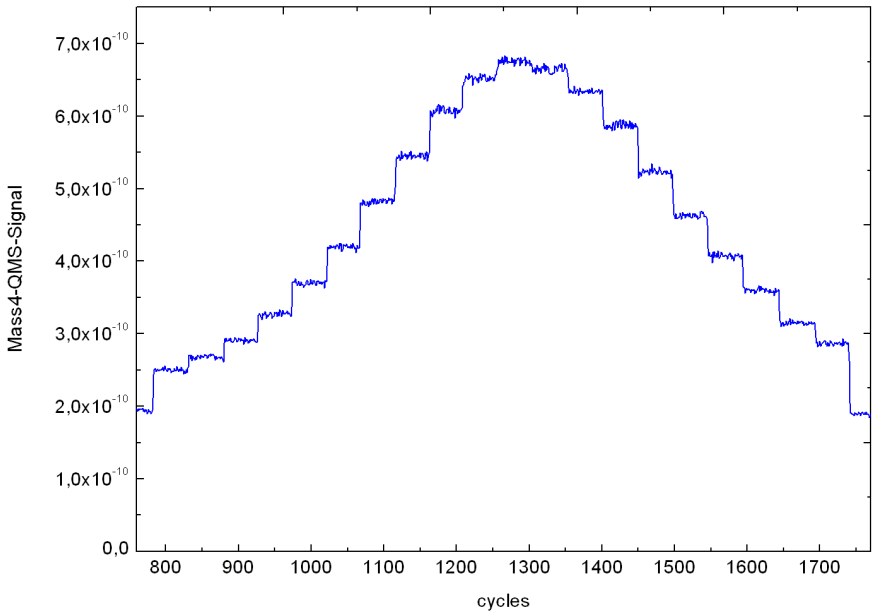

Figure 4.2: Deuterium signal for translational displaced sample. The sample is moved by 2 mm every minute. At the beginning and at the end, one can see the background signal, which has to be subtracted in the analysis.

Possible error sources during the measurements:

- The position of the sample can not be adjusted exactly.
- It is not always easy to determine the exact location of the maximum. This shift varies at different measurements. For most of the measurements, we assumed the maximum to be shifted 1mm to the left.
- The D_2-flux was not constant during the measurements. We noticed that the D_2-flux tended to decrease slightly during time.

4.2 The evaporation process

Clean palladium and palladium with 0.3 MLE VO_x were investigated. This system was extensively studied already by LEED and STM (see[19]-[21]) and the structure was also identified by DFT - calculations (see [22], [23]). To produce the 0.3 MLE VO_x on the palladium surface, an electron beam evaporator was necessary. As described in chap. 3, an oscillating quartz was used to determine the evaporation time. The resulting time was approximately $t = 80$ sec. The vanadium is evaporated at a sample temperature of 523K and at an oxygen pressure of approximately $1 \cdot 10^{-7}$ Torr. Approximately 0.3 MLE VO_x should be on the palladium surface. The monolayer (ML) characterizes the amount of vanadium oxide on the palladium surface. 0.3 MLE VO_x corresponds to a VO_x coverage of 30%.

To verify the amount of evaporated vanadium, AES and LEED can be used.

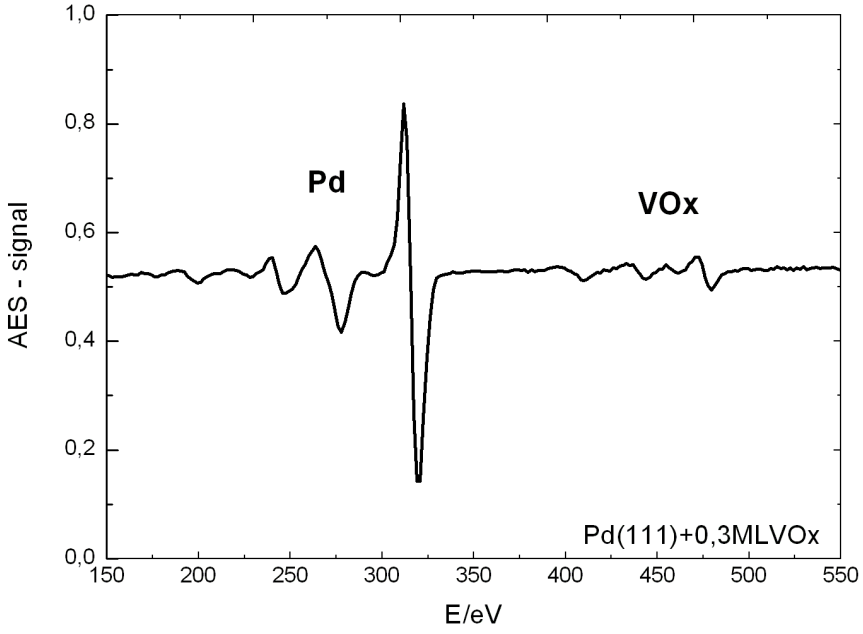

Figure 4.3: AES signal of Pd(111)+0.3 MLE VO_x.

In fig. 4.3, the Auger-spectrum of Pd with 0.3 MLE VO_x is shown.

The structure of the surface adsorbate can be determined from the LEED pattern. The LEED pattern of the clean palladium surface and of palladium + 0.3 MLE VO_x are shown in fig. 4.4 and fig. 4.5. 0.3 MLE VO_x at 523K forms a 2x2 structure.

When considering the corresponding LEED pattern, one can notice that additional reflexes are situated between the main palladium reflexes. The observed LEED pattern is the reciprocal lattice of the real surface lattice (see chap. 3). This 2x2 structure is a surface V_2O_3 phase (see [24]).
The LEED pattern of Pd with 0.3 MLE VO_x changes when the temperature increases. The structure at 700K is shown in fig. 4.6. This structure corresponds to a surface oxide of VO stoichiometry (see [24]).

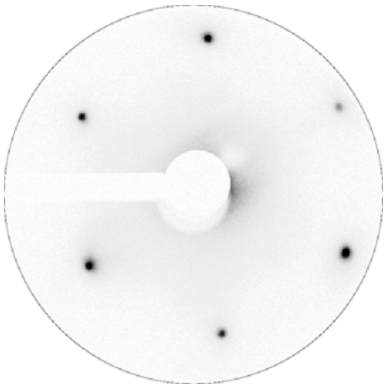

Figure 4.4: LEED picture of clean Pd(111) at 63 eV. This is a 1x1 structure.

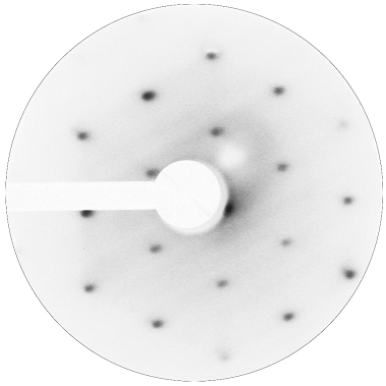

Figure 4.5: LEED picture of Pd(111)+0.3 MLE VO_x at 523K at 63 eV. This is a 2x2 structure. Additional VO_x reflexes are obtained between the main palladium reflexes, as the LEED pattern is the reciprocal structure of the real surface structure. This 2x2 structure corresponds to a V_2O_3 phase on the surface.

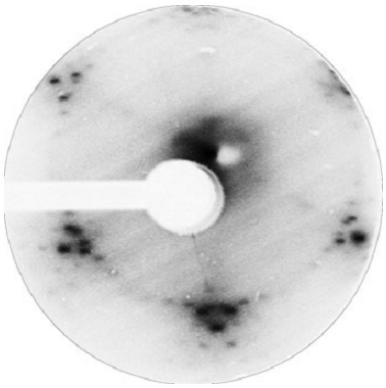

Figure 4.6: LEED picture of Pd(111)+0.3 MLE VO_x at 700K at 63 eV. This structure corresponds to a VO phase on the surface.

4.3 Description of the permeation measurements

The second task of this thesis were permeation measurements on clean Palladium and on Palladium + 0.3 MLE VO_x. One aim of these measurements was to investigate the catalytic effect of Pd(111)+ VO_x to generate water in comparison to the catalytic effect of clean palladium. Clean palladium is a very good catalyst for water production, so the dependance of the water reaction rate on the palladium surface coverage is an interesting task.

In this section, the procedure for the measurements concerning the water formation on palladium is explained.
We call these measurements the 'permeation measurements', but it should be kept in mind that the deuterium is permeated through the palladium sample for the angular distribution measurements as well.

The measurement procedure:

First, the sample is heated at 523K or 700K. During the measurement, the sample holder is LN_2-cooled. Once the sample has reached the desired temperature, the deuterium valve is opened. The deuterium permeates through the palladium sample. The deuterium flux out of the surface increases slowly. One attempts to adjust the deuterium pressure until approximately $p_{HK} = 7 \cdot 10^{-10}$ Torr. When an almost constant deuterium flux is reached, the oxygen valve is opened slowly or in steps. It is important that the oxygen pressure increases slowly, so that the reaction is mostly in equilibrium. The oxygen pressure increases until approximately $p_{HK} = 5 \cdot 10^{-7}$ Torr. Afterwards the oxygen valve is closed slowly again. The whole measurement takes one hour; the procedure of opening and closing the oxygen takes approximately a quarter of an hour. It is important to look after the temperature while measuring, because the reaction rates on the palladium surface depends on temperature. The QMS - signals are saved on a computer.

The more the oxygen-pressure increases, the more water is generated on the palladium surface. Thus, the D_2 - flux decreases. The increase of the oxygen pressure and the corresponding decrease of the deuterium pressure for clean palladium are shown in fig. 4.7.

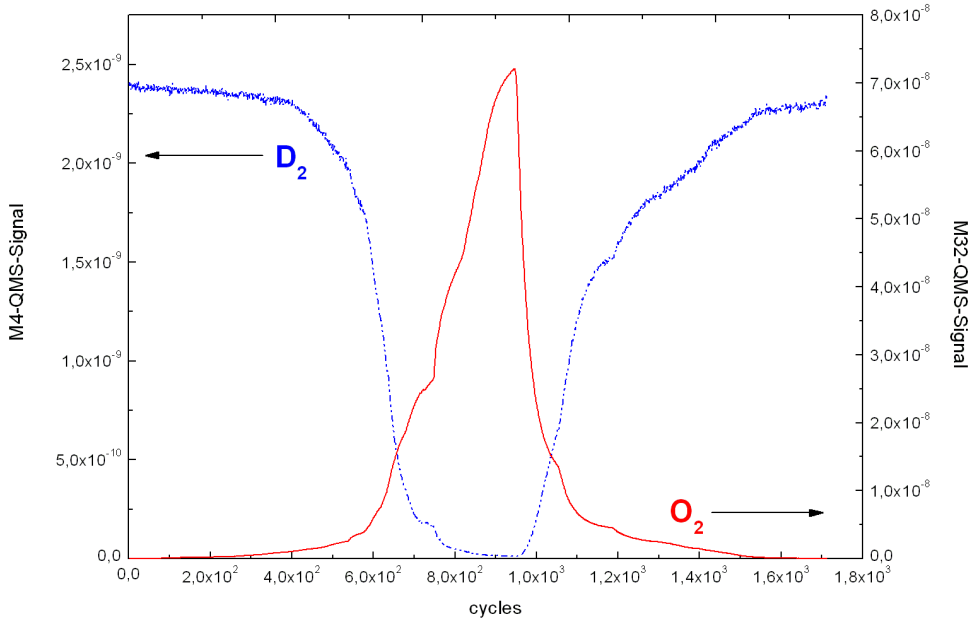

Figure 4.7: The QMS-signal for mass 32 and the QMS - signal for mass 4 are plotted versus the time. The QMS - signal mass 32 corresponds to the oxygen pressure, the QMS - signal for mass 4 corresponds to the deuterium pressure. The measurement was performed on clean Pd(111) at 700K. While the oxygen pressure increases, the deuterium pressure decreases, as oxygen and deuterium react to D_2O.

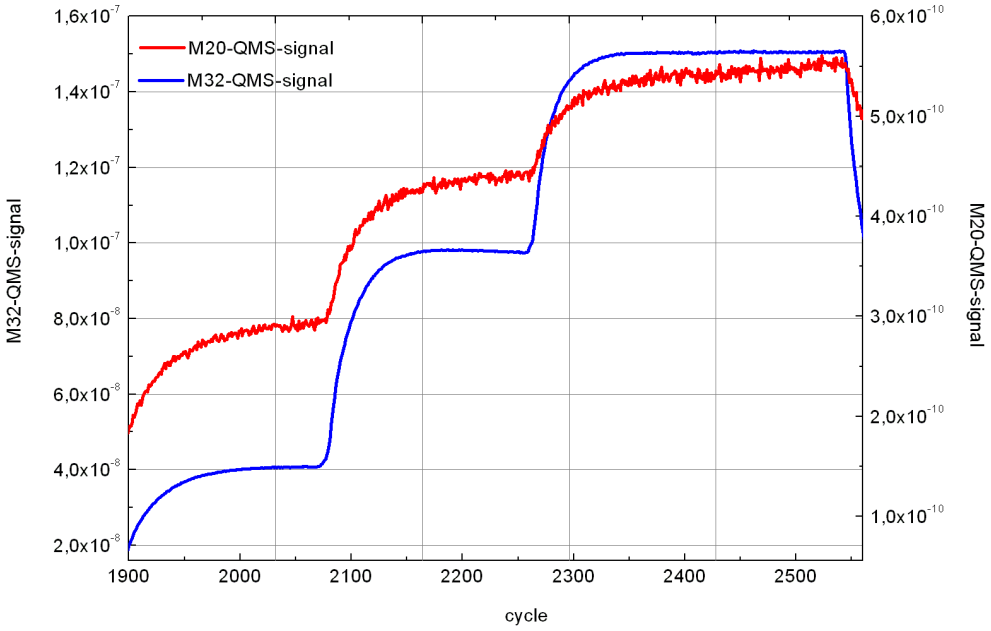

Figure 4.8: The mass 32 QMS - signal and the mass 20 QMS - signal are plotted versus the time. The D_2O pressure slightly increases while the oxygen pressure is constant. It is difficult to determine the moment at which equilibrium is reached. This measurement is performed on Pd(111) + 0.3 MLE VO_x at 523K.

Measurement difficulties:

1. The deuterium valve reacts different at different days. This makes it difficult to compare the measurements with each other. In addition, the respective QMS - factor for D_2O in the detector chamber is not known. One possibility is to consider the D_2 - decrease instead of the D_2O - increase: The respective D_2 - factor of the QMS is well known and the D_2 - decrease can easily be normalized.

2. It seems that the D_2O - production depends not only on the oxygen pressure, but on the oxygen exposition as well. Thus the durability of the 'oxygen - steps' is an important quantity. Considering fig. 4.8, the slight increase of the D_2O-signal during constant oxygen pressure can be seen.
   It has already been mentioned, that it is important to increase and decrease the oxygen pressure slowly. To guarantee that the process is in equilibrium, the way back while turning off the oxygen has been considered. But still, it is important not to proceed too quickly, as can be seen in fig. 4.9. The red line shows the data when

turning off slowly, the blue line is generated when turning off too quickly. It seems to take quite a long time to reach equilibrium conditions.

3. The deuterium flux tends to decrease slowly after some minutes.

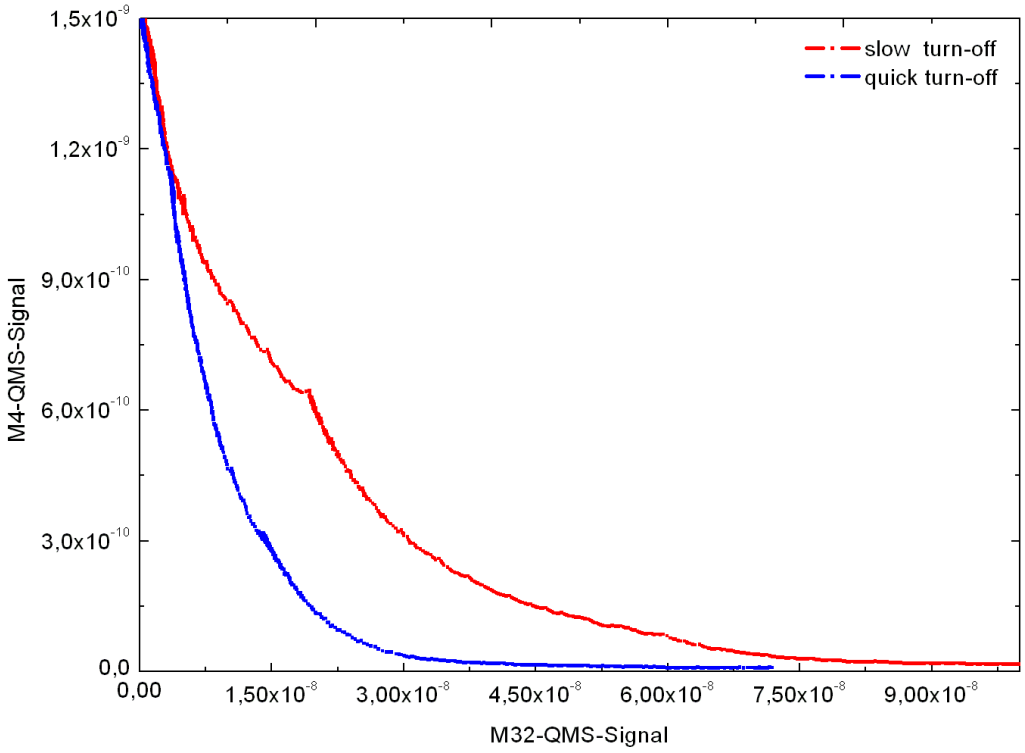

Figure 4.9: The mass 4 QMS - signal is plotted versus the mass 32 QMS - signal. The 'way back' during the decrease of the oxygen pressure is considered. Two different situations are shown: The blue line indicates the deuterium pressure increase when turning off the oxygen quickly. The red line indicates the deuterium pressure increase when turning off slowly. When the oxygen valve is closed too quickly, the deuterium pressure is lower than in case of slow turn - off, as the processes have not enough time to reach equilibrium.

The measurement results for the different situations are described in chap. 7.

Chapter 5

Simulation program for angular desorption distributions

In this chapter, the aim of the program is explained. Two different ways to calculate the fractional amount of detected particles are considered: the analytical way and Monte Carlo simulations. The construction of the simulation program is explained and several examinations of the program are performed. In addition, some simulation results are shown.

5.1 The analytical approach

The simulation program serves to calculate the fractional amount I_0 of particles being detected by a plane detector with radius r_d when I_{ges} particles desorb from the surface of a plane emitter with radius r_e. This calculation can be done analytically or by Monte Carlo simulations.

Although the problem finally has been solved using Monte Carlo simulations, first the analytical way of solving the problem is considered (see [25], [26]):

Assume the angular distribution $J(\vartheta)$ to be (see chap. 2):

$$J(\vartheta) = \frac{n+1}{2\pi} \cdot cos^n\vartheta \tag{5.1}$$

then the flux from a surface element dA_e into a solid angle $d\omega$ at polar angle ϑ is given by:

$$I_{ges}J(\vartheta)dA_e d\omega \tag{5.2}$$

The differential flux from an emitter element dA_e to a detector element dA_d is:

$$d^2I_0 = I_{ges} \cdot J(\vartheta) \cdot \frac{cos\vartheta}{a^2} dA_e dA_d \tag{5.3}$$

a...distance between emitter and detector element.

By integrating, one gets thus:

$$I_0 = I_{ges} \int_0^{r_d} \int_0^{r_e} \int_0^{2\pi} \int_0^{2\pi} \frac{J(\vartheta)}{a^2} \cdot cos\vartheta \cdot \rho_e \cdot \rho_d, d\varphi d\psi d\rho_e d\rho_d \tag{5.4}$$

ρ_e is the distance between center point of emitter and desorbing point of the emitted particle, ρ_d is the distance between center point of the detector and arrival point of the detected particle. One has to integrate over the whole emitter plane with radius r_e and the whole detector plane with radius r_d. When considering fig. 5.1 one can find the following equation for a:

$$a^2 = \rho_e^2 + \rho_d^2 - 2\rho_e\rho_d cos(\psi - \varphi) + d^2 \tag{5.5}$$

$$d = a \cdot cos\vartheta \tag{5.6}$$

is the orthogonal distance between the emitter plane and the detector plane.

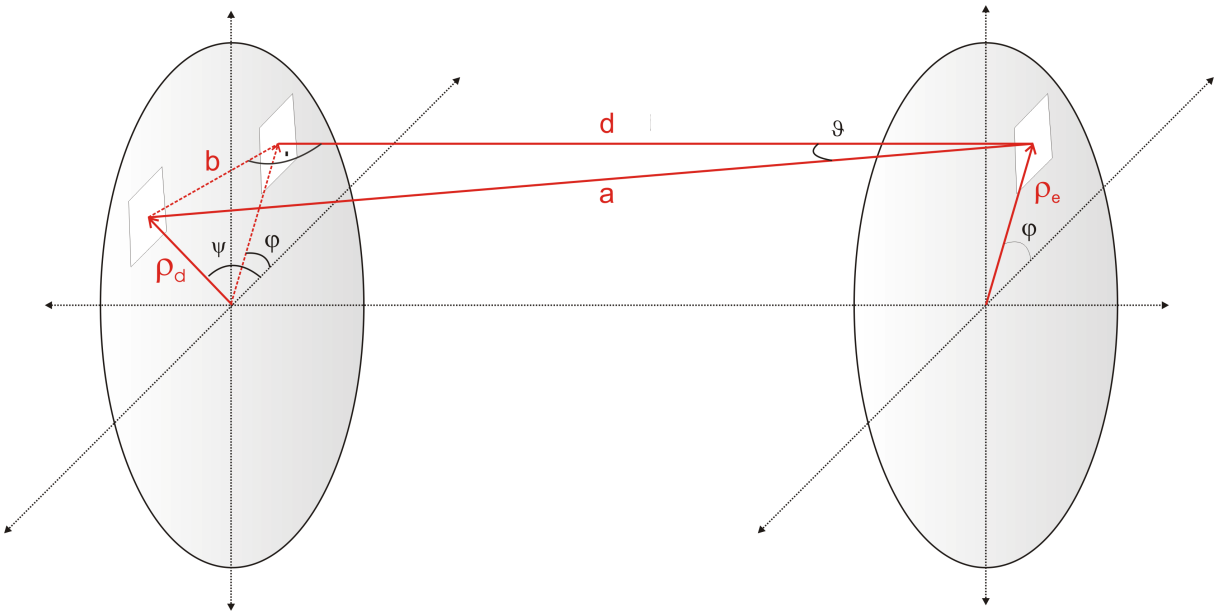

Figure 5.1: Geometrical considerations concerning the distances and angles in the emitter - detector system. The total distance a between desorption point and arrival point can be calculated using the law of cosine and the law of Pythagoras.

Since

$$\frac{I_0}{I_{ges}} = \frac{n+1}{2\pi} \int_0^{r_d} \int_0^{r_e} \int_0^{2\pi} \int_0^{2\pi} \frac{d^{n+1}}{a^{n+3}} \cdot \rho_e \cdot \rho_d \, d\varphi d\psi d\rho_e d\rho_d \tag{5.7}$$

we get

$$\frac{I_0}{I_{ges}} = \frac{n+1}{2\pi} \int_0^{r_d} \int_0^{r_e} \int_0^{2\pi} \int_0^{2\pi} \frac{d^{n+1}}{(d^2 + \rho_e^2 + \rho_d^2 - 2\rho_e\rho_d cos(\psi - \varphi))^{\frac{n+3}{2}}} \rho_e\rho_d \, d\varphi d\psi d\rho_e d\rho_d. \tag{5.8}$$

When the detector and the emitter are parallel and the two have their center point in the z-axis, the integral can be reduced to a threefold integral because of the azimuth symmetry (see [25]):

$$\frac{I_0}{I_{ges}} = (n+1) \cdot d^{n+1} \int_0^{r_d} \int_0^{r_e} \int_0^{2\pi} \frac{\rho_e \cdot \rho_d}{(d^2 + \rho_{et}^2 + \rho_d^2 - 2\rho_e\rho_d cos(\psi - \varphi))^{\frac{n+3}{2}}} \, d\varphi d\rho_e d\rho_d \tag{5.9}$$

5.2 Monte Carlo simulations

Another approach to solve the problem are Monte Carlo simulations:
The paths of I_{ges} randomly generated particles are considered. It is examined if the particles are detected or not. In case of large values of I_{ges}, the intensity ratio gained by simulations is a good approximation for the real value of the intensity ratio. We proceed in the following manner:

An element on the emitter plane is randomly selected as starting point. The polar angle ϑ and the azimuthal angle φ are randomly determined according to the $cos^n\vartheta$ - distribution and the consequential arrival point in the detector plane is calculated. Finally, each particle lying on the detector surface is counted.

We were interested essentially in three configurations:

- The emitter and the detector are parallel. The distance d between them can be changed.
- The emitter is shifted in one direction parallel to the detector, while the normal distance between detector plane and emitter plane remains the same.
- The emitter is tilted by the angle α. This is equivalent with moving the detector on a semicircle by the angle α.

These situations can easily be simulated by Monte Carlo simulations, as will be explained in the next section. By contrast, the analytical way is more complicated. The simplification leading to (5.9) can not be done anymore, so the fourfold integral has to be solved. Thus, Monte Carlo methods have been used to solve the problem.

5.2.1 Design of the simulation program

We design the simulation program in four steps:

1. **Determination of a random point on the emitter.**

   Uniformly distributed random points are generated on a rectangular emitter with side lengths a and b or on a circular emitter with radius r_e using cartesian coordinates.

2. **Generation of the angles ϑ and φ.**

   We generate the angles ϑ and φ similar to [27] and [28]:
   Again, we assume the particles to leave the surface according to the cosine distribution. Thus, we get for the number dn of desorbing particles in the solid angle $d\omega$:

   $$\frac{dn}{d\omega} = I_{ges} \cdot \frac{n+1}{2\pi} \cdot cos^n\vartheta \tag{5.10}$$

   Using spherical coordinates, $d\omega$ can be expressed by:

   $$d\omega = sin\vartheta d\vartheta d\varphi \tag{5.11}$$

   ϑ is the polar angle, i.e. the angle to the normal of the surface. φ is the azimuthal angle, that is the angle between the projection of the particles direction in the x-y-plane and the x-axis. (see fig. 5.2)

   The values of the azimuthal angle φ are uniformly distributed in the interval $(0,2\cdot\pi]$. To generate a value for φ, a random number r in the interval (0,1] is chosen and φ is obtained by $\varphi = r \cdot 2 \cdot \pi$.

   To gain a value for ϑ, it is first necessary to calculate the polar-angle probability function $f(\vartheta)$ by integrating eq.(5.10) with respect to φ:

   $$\frac{dn}{d\vartheta} = I_{ges} \cdot \frac{n+1}{2\pi} cos^n\vartheta sin\vartheta \int_0^{2\pi} d\varphi. \tag{5.12}$$

   That gives:

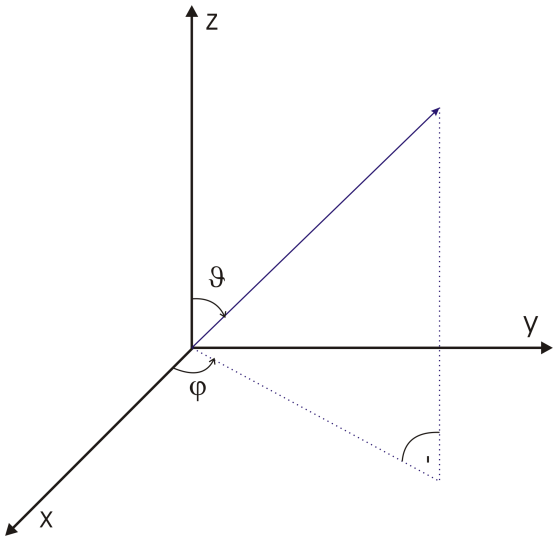

Figure 5.2: Illustration of the polar angle ϑ and the azimuthal angle φ: We assume the emitter to be in the $x-y$ plane. Thus, ϑ is the angle between the emission vector and the emitter normal vector, φ is the angle between projection of the emission vector in $x-y$ plane and the x - axis

$$f(\vartheta) = \frac{1}{I_{ges}} \cdot \frac{dn}{d\vartheta} = (n+1) \cdot cos^n \vartheta sin\vartheta \tag{5.13}$$

Since

$$\int sin(x)cos^n(x)dx = -\frac{1}{n+1} \cdot cos^{n+1}x \tag{5.14}$$

it is possible to obtain the angle ϑ by a random number r in the range (0,1) via

$$r = \frac{\int_0^{\vartheta} f(\vartheta)d\vartheta}{\int_0^{\pi/2} f(\vartheta)d\vartheta} = 1 - cos^{n+1}\vartheta. \tag{5.15}$$

Thus

$$\vartheta = acos\ \sqrt[n+1]{1-r} \tag{5.16}$$

3. **Calculation of the arrival point.**

The arrival point of the particle on the detector is calculated according to the geometry of the emitter - detector system.

ad a) *Emitter and detector are parallel and the distance between them varies.*

As the emitter is parallel to the detector, the total distance a from the emitter point to the arrival point is given by:

$$a = \frac{d}{cos\vartheta} \tag{5.17}$$

It is possible to describe the arrival point by spherical coordinates and shifted cartesian starting points:

$$x_d = a \cdot sin\vartheta \cdot cos\varphi + x_e \tag{5.18}$$

$$y_d = a \cdot sin\vartheta \cdot sin\varphi + y_e \tag{5.19}$$

$$z_d = a \cdot cos\vartheta \tag{5.20}$$

ad b) *The emitter is shifted in one direction parallel to the detector, while the normal distance between emitter and detector remains the same.*

(5.17) is valid, as emitter and detector are still parallel. The arrival point is calculated similar as in (5.18), but the length of the displacement has to be added to the x-coordinate of the arrival point.

ad c) *The emitter is tilted by an angle α.*

(5.17) is not valid in case of tilt of the emitter plane, as the detector and the emitter planes are not parallel anymore, so we have to proceed in a different manner. A simplification can be done by considering instead of a tilted emitter the following, equivalent situation:

The emitter is fixed and the center point of the detector is shifted on a semicircle around the emitter, which lies in the middle of the semicircle. This situation can easily be solved (see fig. 5.3).

The equation of a plane in three-dimensional space is generally given by

$$\frac{x}{l} + \frac{y}{m} + \frac{z}{n} = 1 \tag{5.21}$$

where l, m and n are the respective axis intercepts. For the plane containing the detector area we have $m = \infty$, as we shift the detector around an axis around the y - direction. From fig. 5.3 we see

$$n = \frac{d}{cos\alpha} \tag{5.22}$$

and

$$l = \frac{d}{sin\alpha} \tag{5.23}$$

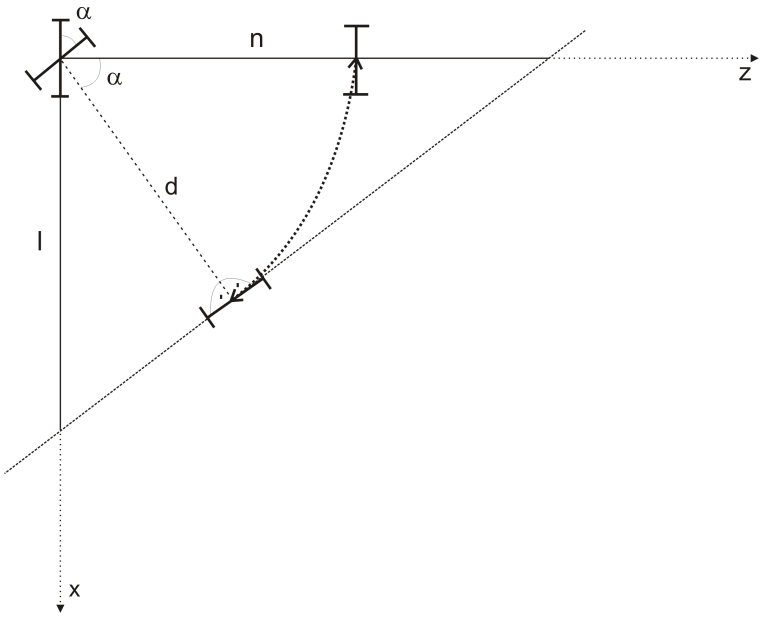

Figure 5.3: The center point of the detector is shifted on a semicircle around the y-axis. Thus the geometrical considerations are done in the x-z-plane. Using the law of Pythagoras, the axis intercepts n and m can be calculated

Thus, the equation of the detector plane is:

$$\frac{sin\alpha \cdot x}{d} + \frac{cos\alpha \cdot z}{d} = 1 \tag{5.24}$$

The coordinates of a point with origin $[x_e, y_e, 0]$ are generally given by (5.18). We use the unknown distance a as a parameter. Thus, we get four equations with four unknown parameters. So it is possible to get a formula for the distance a:

$$a = \frac{1 - \frac{sin\alpha \cdot x_e}{d}}{\frac{sin\alpha \cdot sin\vartheta \cdot cos\varphi}{d} + \frac{cos\alpha \cdot cos\vartheta}{d}} \tag{5.25}$$

To calculate the coordinates of the arrival point we use again (5.18), where the distance a is calculated by (5.25).

4. **Selection of arrival points on the detector.**

   To determine the detected particles, the distance r from the arrival point to the center point of the target is calculated

$$r = \sqrt{(x_d - x_{center})^2 + (y_d - y_{center})^2 + (z_d - z_{center})^2} \tag{5.26}$$

   and the particles whose distance r is not greater than the detector radius r_d are counted.
   In case of a rectangular detector, each coordinate of the arrival point is compared with the respective detector length. If none of the coordinates lies outside the detector, the particle is considered as detected.

5.2.2 Testing the program

Several tests have been performed to verify the results of the simulation program.

Examination of the generated angles

It is easy to examine the generated angular distributions. To simulate an isotropic direction distribution in the R^3

- the angle φ has to be uniformly distributed in the interval $[0, 2\pi]$;
- the cosine of the angle ϑ has to be uniformly distributed in the interval $[-1, 1]$ (see [29]).

Considering the angular distribution in a hemisphere, we expect $cos\vartheta$ to be in the interval $[0, 1]$.

Using the following small test program we check if the cosines of the simulated values of ϑ are uniformly distributed in [0,1]. The result is shown in fig 5.4.

```
%Examination of the generation of the angular distribution

thetavec=zeros(0);

nexp=0;

for index=1:10000

            exponent=1/(nexp+1);
            theta(index)=acos((1-rand)^exponent);

end

%!! The cosine has to be uniformily distributed
thetavec=cos(theta); hist(thetavec,20);
```

The algorithm obviously produces angles ϑ which obey the cosine distribution.

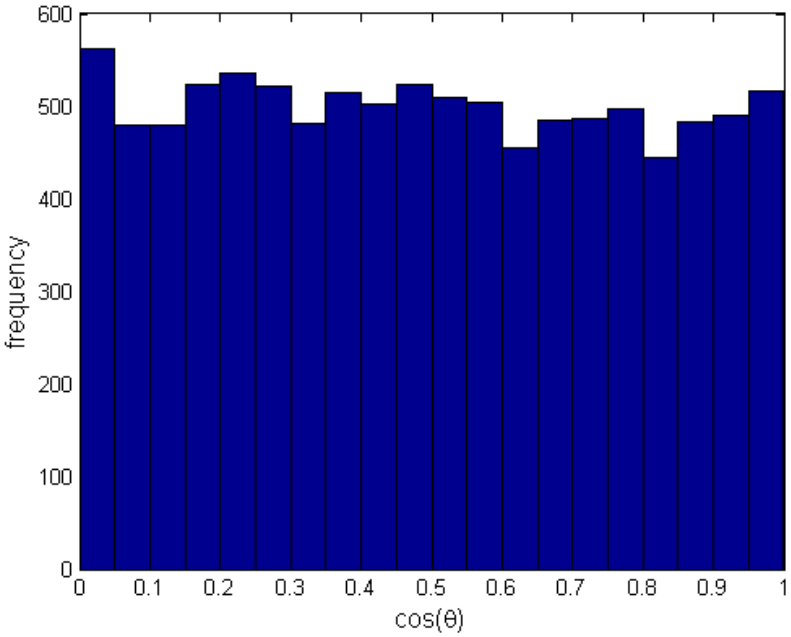

Figure 5.4: Examination of the generated angular distribution: the cosine of the generated ϑ-values has to be uniformly distributed in the interval [0,1]. The figure shows the output of the test program.

Comparison of our results with earlier performed calculations

Furthermore, the data produced by changing the distance between detector and emitter have been compared to an earlier performed calculation (see [26]). In this thesis, calculations have been done for a rectangular $10mm$ x $10mm$ emitter and a circular detector with radius $r_d = 2.5mm$. The simulations were performed using these parameters. The sample and the detector are parallel and the respective center points are on the same axis. The distance between detector and emitter is varied. The results are similar to the calculation results done by [26], as shown in fig. 5.5:

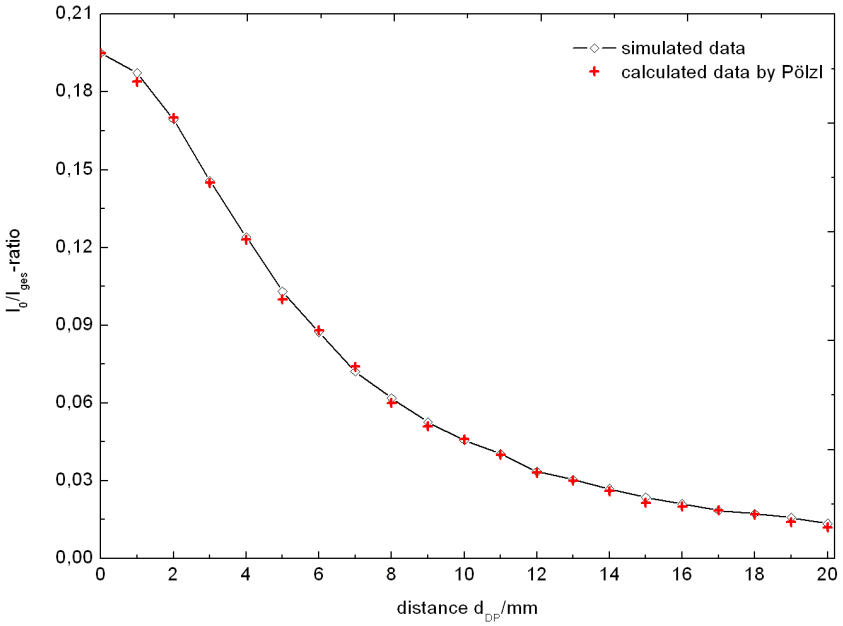

Figure 5.5: Calculation of detected particle ratio I_0/I_{ges} as a function of the distance d. Comparison with an earlier performed calculation for an rectangular 10 mm x 10 mm emitter and a circular detector with radius $r_d = 2.5$ mm. The black line shows the simulation result, the red crosses are the results of the calculation. The simulated data correspond very well to the calculated data.

Examination of the program in case of a tilted emitter

The results obtained by tilting the emitter can be verified by considering two extreme situations:

1. *Small emitter radius r_e, large detector radius r_d and small distance d between detector and emitter:*

   The resulting function should slowly decrease. For $\alpha = \pi/2$, approximately 50% of the particles should be detected.

2. *Large emitter radius r_e, small detector radius r_d and sufficiently large distance d between detector and emitter:*

   – For $n = 0$, i.e. the same number of emitted particles in every direction, the resulting function should increase with increasing angle α, because the accessible surface increases. For angles near $\alpha = \pi/2$, the number of detected particles

decreases by geometric reasons.

– For $n = 1$, the output graph should be constant. The increase caused by the larger accessible surface is compensated by the decrease due to the cosine distribution. Again, for angles near $\alpha = \pi/2$ the detector surface within reach becomes smaller.

The results of the simulation for these different situations are shown in fig 5.6 and fig 5.7:

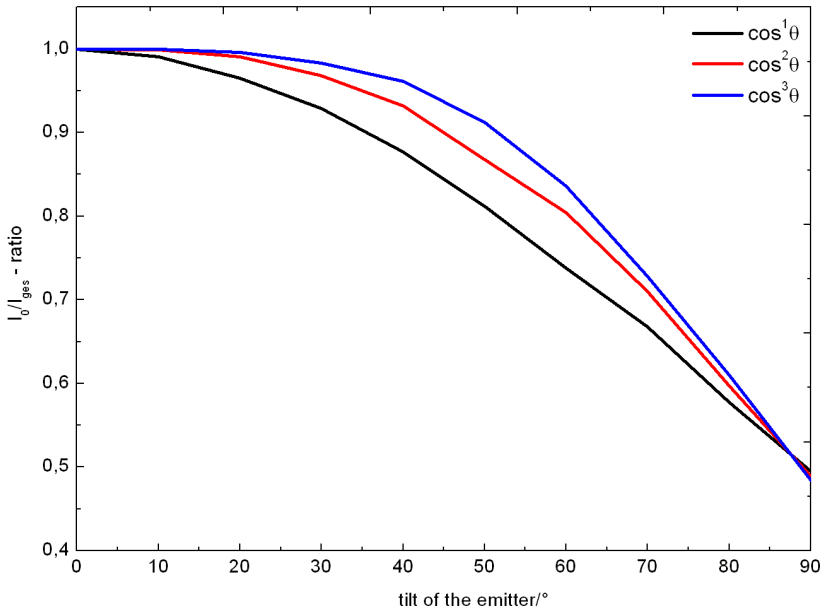

Figure 5.6: Simulation result for case 1. The following input parameters have been used: r_e=1, r_d=100, d=1.5. For α=$\pi/2$, approximately 50% of the particles are detected.

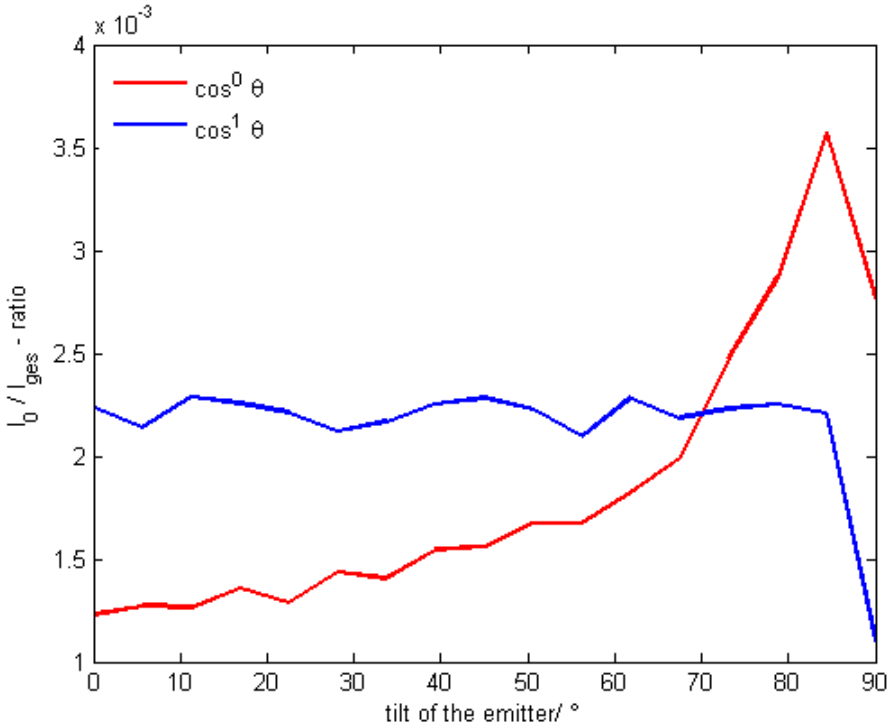

Figure 5.7: Simulation result for case 2. The following input parameters have been used: r_e=30, r_d=2, d=30. Again when approximating to $\alpha=\pi/2$, the number of detected particles decreases.

The reliability of the simulation results

When performing Monte Carlo simulations, it is also necessary to think about the reliability of the simulated data. We need a sufficiently great number of particles to obtain plausible results without much noise. It is not possible to designate a certain number of particles which have to be emitted at least, because the noise of the data depends on the number of detected particles. This in turn depends on the radius of the emitter and the detector and on the distance between them.
In addition, results for two different configurations are shown. In both cases, the number of emitted particles $I_{ges} = 100000$, but as the parameters are chosen in a different way, in the second case the data shows much more noise:

In fig. 5.8, the following parameters have been used:

Radius of the emitter $r_e = 5$
Radius of the detector $r_d = 10$
Distance d between detector and emitter varies from $d = 0$ to $d = 20$

In fig. 5.9, the following parameters have been used:

Radius of the emitter $r_e = 30$
Radius of the detector $r_d = 1$
Distance d between detector and emitter varies from $d = 0$ to $d = 20$

As one can see, although the number of emitted particles I_{ges} is the same in both cases, the graph in fig.5.9 shows much more noise than the graph in fig.5.8. Of course, also the distance dependance changes due to the different geometries.

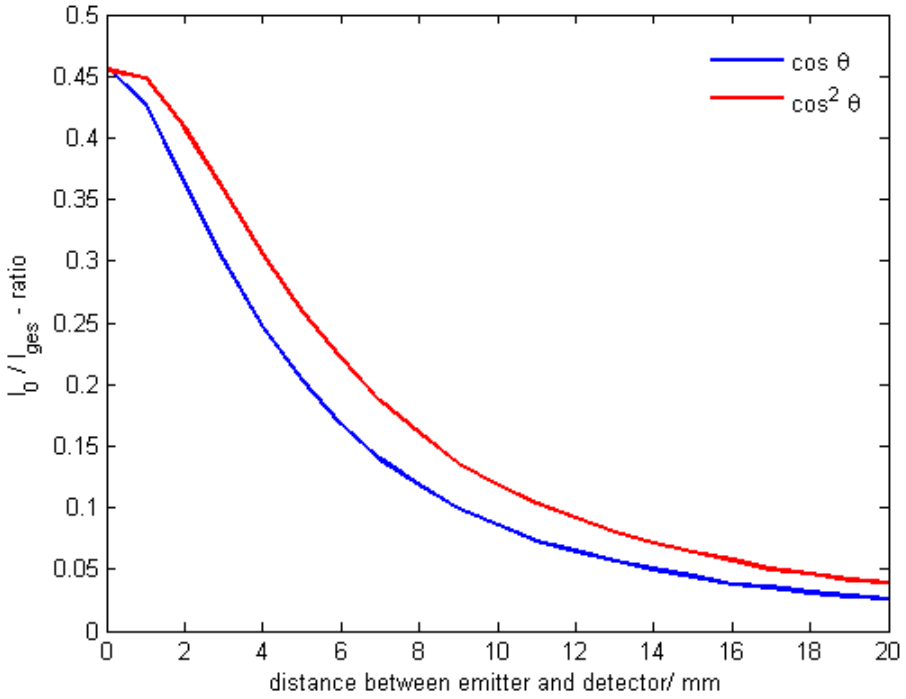

Figure 5.8: Ratio of detected particles in dependence of the distance. I_{ges}=100000 particles are desorbing. As the detector is larger than the emitter, many particles are detected, whereby little noise is produced.

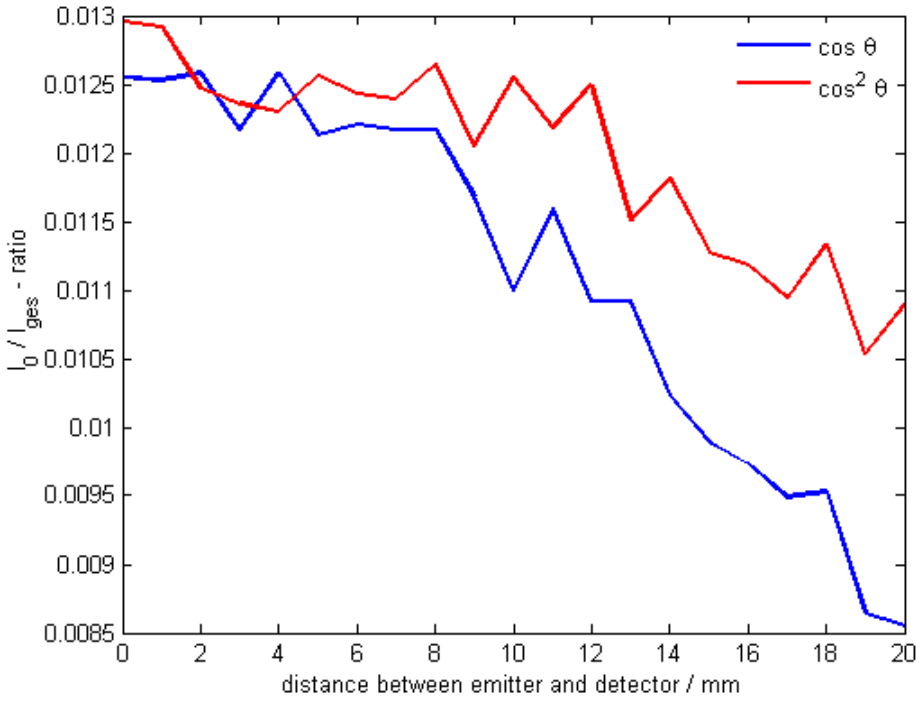

Figure 5.9: Ratio of detected particles in dependence of the distance. I_{ges}=100000 particles are desorbing. The emitter is larger than the detector: Few particles are detected so much noise is produced.

5.2.3 Simulation results

In addition, some results of the simulation program for shifted and tilted emitter using typical parameters are presented:

- **An example for shifted emitter:** (See fig. 5.10)
  Radius of the emitter $r_e = 4$
  Radius of the detector $r_d = 3.5$
  Distance between detector and emitter $d = 12$.

- **An example for tilted emitter:** (See fig. 5.11)
  Radius of the emitter $r_e = 4$
  Radius of the detector $r_d = 4$
  Distance between detector and emitter $d = 10$.

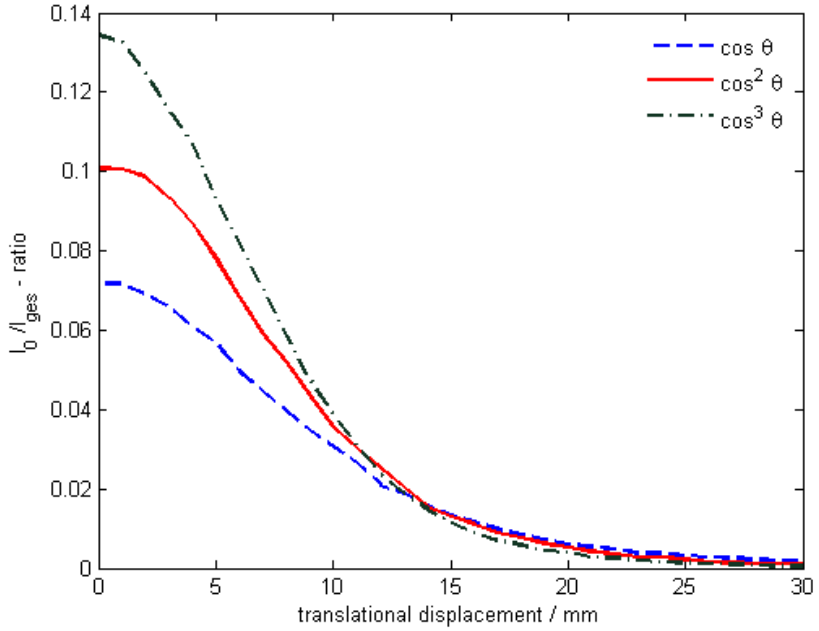

Figure 5.10: Simulation result in case of translational displacement of the emitter. Typical input parameters: r_e=4, r_d=3,5 and d=12. The ratio of detected particles in dependance of the displacement is shown.

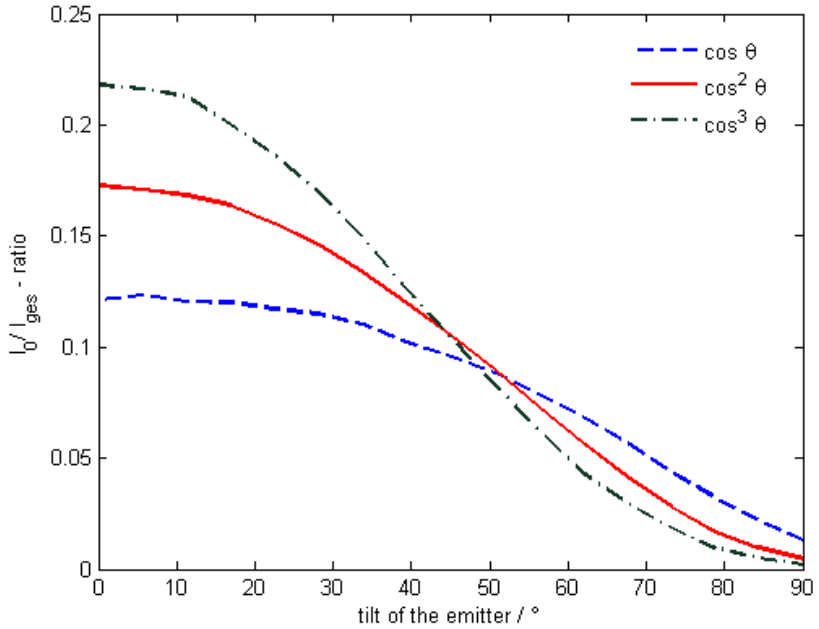

Figure 5.11: Simulation results in case of a tilted emitter for typical input parameters r_e=4, r_d=4 and d=10. The ratio of detected particles in dependance of the tilting of the emitter is shown.

Chapter 6

Comparison of simulation results and measurements

In this chapter, the measured angular distributions of deuterium desorbing from the palladium surface are shown. The measured data are compared with the simulation results and a guess for the respective $cos^n\vartheta$-distribution is given. Furthermore, the resulting dependance of the angular distributions from the temperature is compared with the energy dependance of the sticking coefficient of deuterium.

6.1 Comparison of measured angular distributions with simulation results

Several angular distribution measurements have been performed in the way as described in chap. 4. The angular distribution of deuterium desorbing from clean palladium and from vanadium- and potassium covered palladium were measured at two different temperatures by displacing the sample in front of the detector, as described in chap. 4.
The following measurements were compared with the simulated results:

1. clean Pd(111) at 523K and at 700K
2. Pd(111) with 0.3 MLE vanadium oxide at 523K and at 700K
3. Pd(111) with 0.2 ML potassium at 523K

The simulation was performed for the following case:
Detector and emitter are parallel and the emitter is displaced in one direction parallel to the detector. The normal distance between detector plane and emitter plane remains the same.

The input parameters were chosen according to the measurement geometry. We assumed the radius of the effective desorbing palladium sample to be smaller than the whole sample radius assigned in chap. 3.

Radius of the emitter: $r_e = 3.5$
Radius of the detector: $r_d = 4$
Distance between sample and detector: $d = 17$

For each simulation, the number of emitted particle is $I_{ges} = 100000$

ad 1)

The angular distributions of deuterium desorbing from clean Pd(111) were measured at 523K and at 700K. The resulting data are shown in fig. 6.1. As shown in chap. 4, it is not possible to determine the exact position of the maximum, as the measured angular distributions exhibit a small asymmetry. The sample was moved in steps of 2 mm, therefore we assumed the right position of the maximum to be shifted by 1 mm.

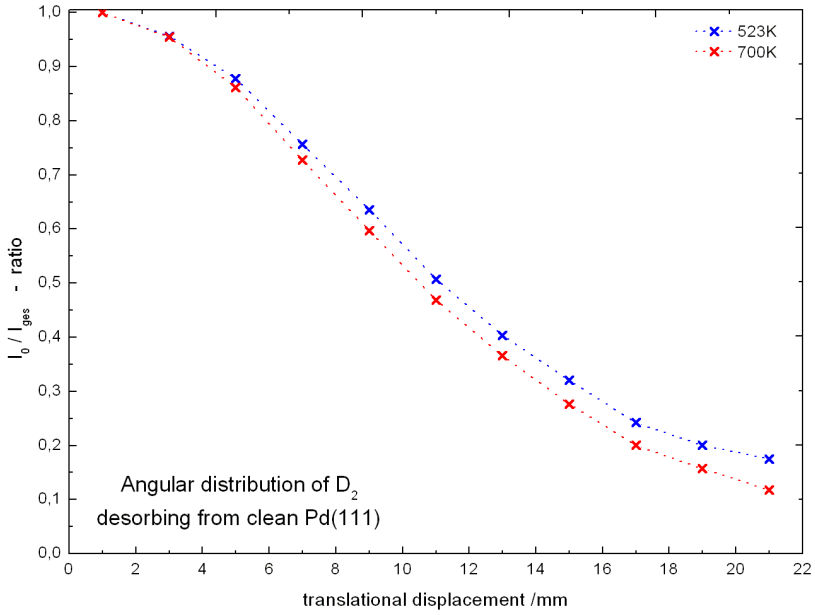

Figure 6.1: The measured angular distributions for deuterium desorbing from clean Pd(111) at 523K and 700K are shown. The data are normalized so they are comparable to the simulation results. At zero position, the sample holder seems not to be directly in front of the detector, so the intensity maximum is displaced by 1 mm.

The measured data were compared with the simulated data. It seems that clean Pd(111) at 523K has a $cos-$distribution, as shown in fig. 6.2. This fits quite well to earlier performed measurements, for example described in [30].

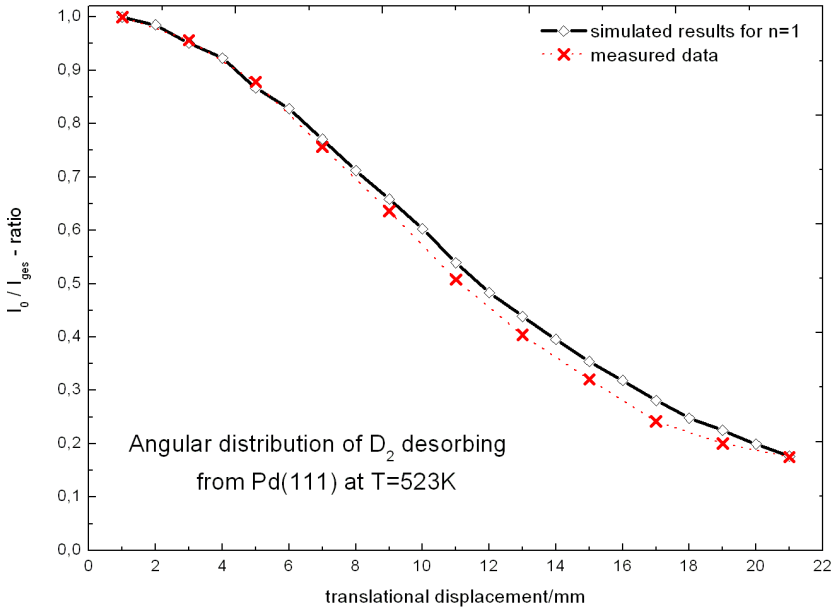

Figure 6.2: The red crosses show the measured angular distribution of clean Pd(111) at 523K. The black line is the simulation result for $cos-$distribution. The measured data correspond quite well to the simulated data.

The measured angular distribution of deuterium desorbing from clean Pd(111) at 700K is sharper than the angular distribution of deuterium desorbing from clean Pd(111) at 523K. There is a good agreement with the simulation data for a cos^2-distribution, as is shown in fig. 6.3.

During measurements, several sources of errors may occur, as mentioned already in chap. 4. The sample position can not be adjusted exactly and it is difficult to determine the exact location of the maximum. In addition, the deuterium flux tends to decrease slightly after time. Besides, when analyzing the data, a mean value of the measured data was estimated at each step, which may produce a small error as well. Taking into account all these mentioned possible error sources, the measured angular distribution seems to fit well to the expected cosine distributions.

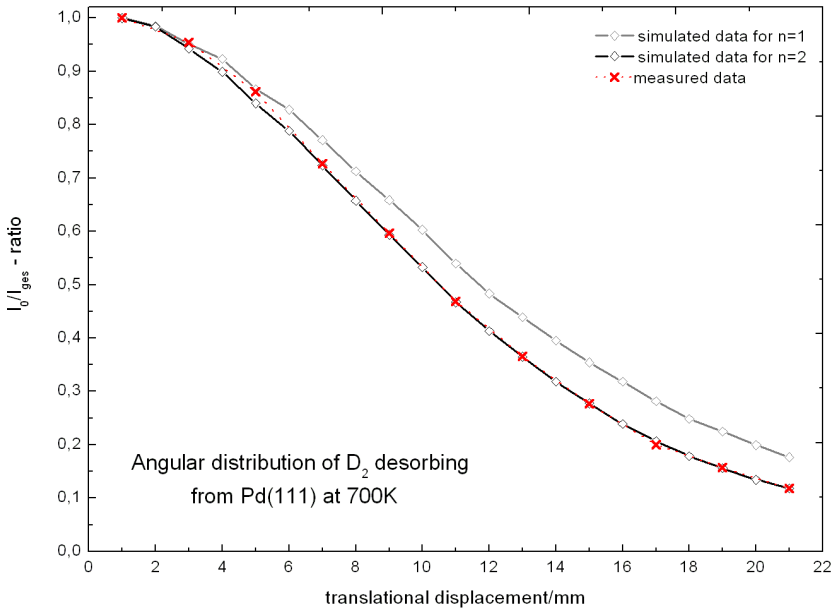

Figure 6.3: The red crosses show the measured angular distribution of clean Pd(111) at 700K. The black line is the simulation result for a cos^2-distribution. The measured data correspond very well to the simulated data.

ad 2)

The angular distribution of Pd(111) + 0.3 MLE VO_x was measured at two different temperatures. There seems to be not much difference between the angular distribution of deuterium desorbing from Pd(111)+0.3 MLE VO_x and from clean Pd(111). In fig. 6.4 and fig. 6.5, the angular distributions corresponding to clean palladium and to palladium with 0.3 MLE VO_x at the respective temperatures are shown. The angular distribution of deuterium desorbing from Pd(111)+0.3 MLE VO_x seems to be a little bit sharper than the angular distribution of clean Pd(111).

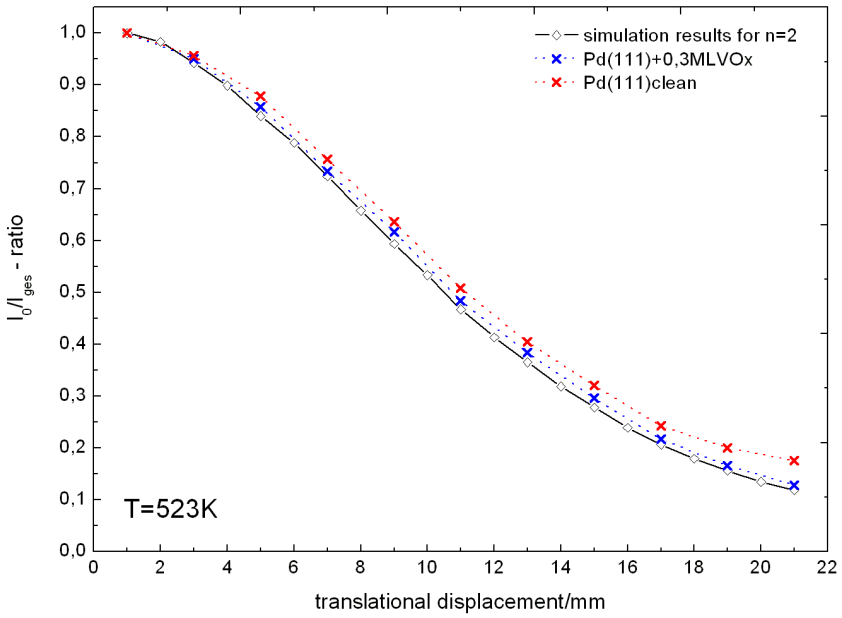

Figure 6.4: The measured angular distribution of desorbing deuterium from clean Pd(111) and Pd(111)+0.3 MLE VO_x at 523K, respectively, are shown. There is not much difference between the distributions even though the angular distribution of vanadium covered palladium seems to be a little bit sharper. For comparison, the simulation result for $cos^n\vartheta$ - distribution is shown. The angular distribution of Pd(111) + 0.3 MLE VO_x seems to have a value of n between $n = 1$ and $n = 2$.

ad 3)

Finally, the palladium surface has been evaporated with potassium and the angular distribution has been measured at 523K. The angular distribution of deuterium desorbing from potassium covered palladium, Pd(111)+K, is sharper than the distribution of clean palladium. In fig. 6.6, the angular distributions of deuterium desorbing from clean Pd(111) and Pd(111)+K are compared with the simulated angular distributions. The angular distribution of Pd(111)+K seems to fit very well the cos^3-distribution.

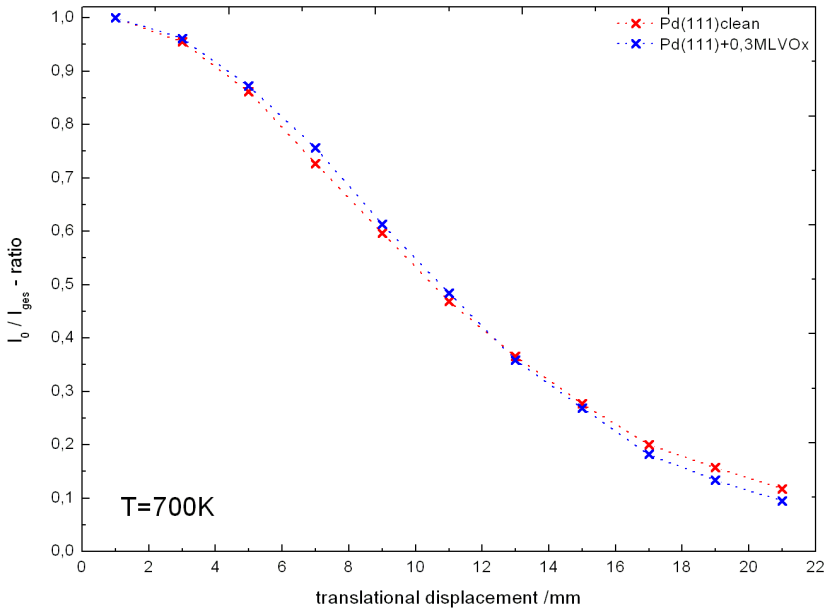

Figure 6.5: The measured angular distribution of clean Pd(111) and Pd(111)+0.3 MLE VO_x at 700K are compared. Although the shape of the distributions looks a little bit different, it is not possible to determine if one of them is sharper than the other.

6.2 Comparison of the measured sticking coefficient with the angular distributions

A further interesting task is to compare the measured angular distributions with the energy dependance of the sticking coefficient. In [1], the energy dependance of the initial sticking coefficient $S(E)$ for deuterium adsorbing on Pd(111) has been measured (see fig. 6.7):
After a short decrease at low energies, the sticking coefficient is increasing. The decrease of the sticking coefficient at low energies is a strong indicator for a precursor path. This is quite unusual, as for the systems Ni(111) and Pt(111) which are in the same group in the periodic table, only a direct adsorption path exists (see [18]). An alternative way to describe the decrease of the sticking coefficient at low energies are steering effects, as mentioned in chap. 2.

At high energies, the sticking coefficient increases. This indicates an activation barrier in the chemisorbed state. The increase of the sticking coefficient at high energies corresponds to an angular distribution sharper than cosine, if one assumes normal energy scaling to be valid.
As the maximum of the Maxwell Boltzmann distribution is shifted to higher energies for

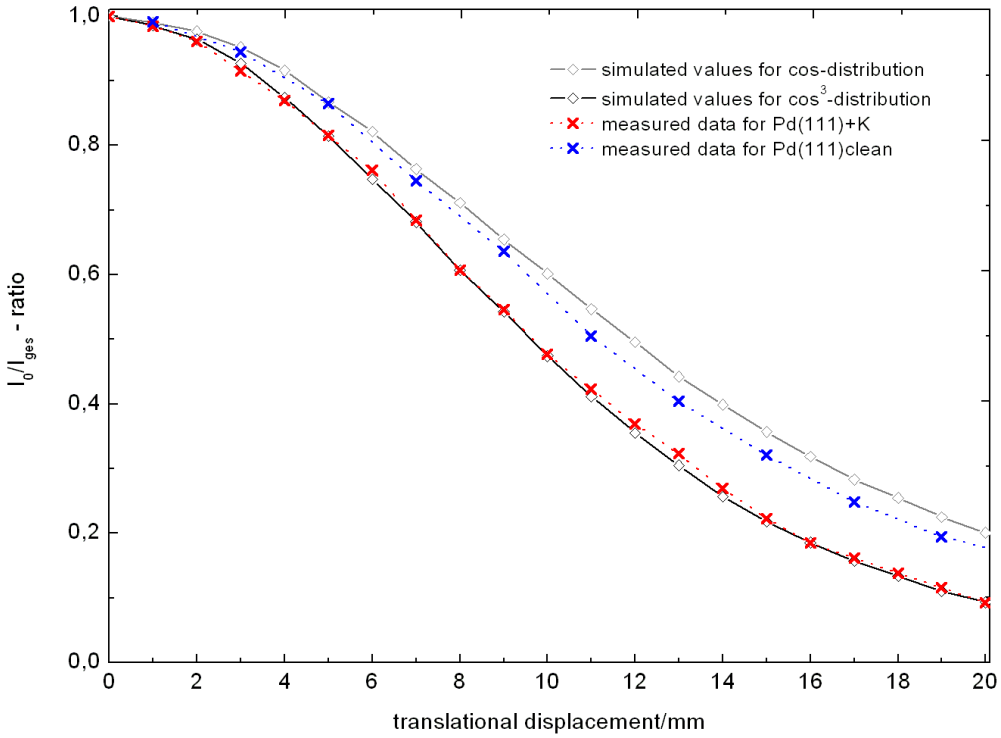

Figure 6.6: The measured angular distribution of deuterium from clean Pd(111) and Pd(111)+ 0.2 ML K at 523K are shown (red and blue crosses). The black line is the simulation result for *cos*-distribution, the dashed line is the simulation result for cos^3-distribution. The angular distribution of deuterium desorbing from potassium covered palladium fits very well to the cos^3-distribution.

high temperatures (see fig. 6.8), we expected to be able to approve our angular distribution measurements and to get sharper angular distribution in case of 700K than in case of 523K.

We have to take into account that the measured values for the sticking coefficient are gained by an experiment which used a monoenergetic beam. Desorbing particles in our experiment are assumed to have energies according to the Maxwell-distribution:

$$N_T(E) \sim E \cdot e^{(-\frac{E}{kT})} \tag{6.1}$$

The sticking coefficient at a certain temperature T is thus given by:

$$S_T = \frac{\int N_T(E) \cdot S(E)\, dE}{\int N_T(E)\, dE} \tag{6.2}$$

As normal energy scaling is assumed to be valid,

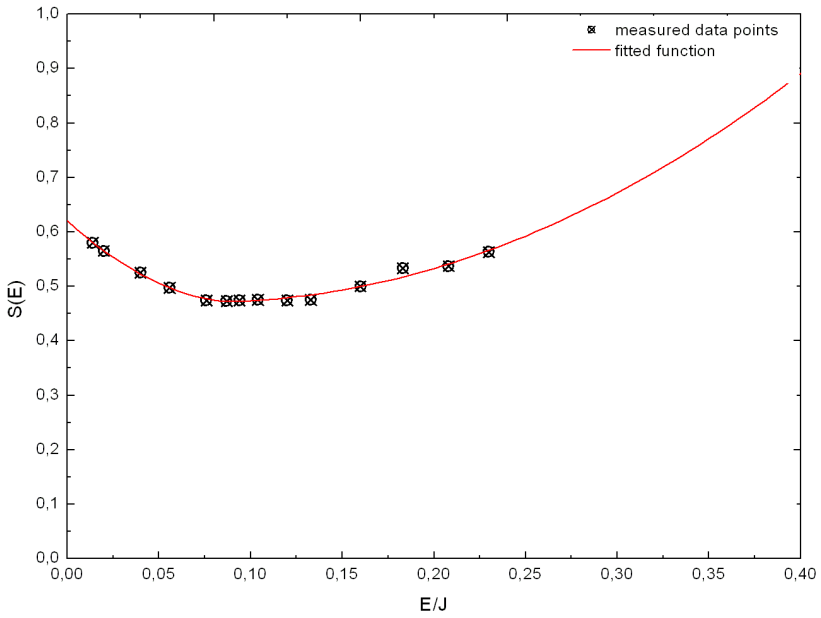

Figure 6.7: The black points show the measured value for the sticking coefficient S of deuterium in dependence of the beam energy E from [1]. The red line is the fitted function: it consists of two polynomials.

$$E_{\perp}(\vartheta) = E_0 \cdot cos^2\vartheta$$

it follows that

$$S_T(\vartheta) = \frac{\int N_T(E/cos^2\vartheta) \cdot S(E)\, dE}{\int N_T(E/cos^2\vartheta)\, dE} \tag{6.3}$$

First, it was necessary to get a function $S(E)$ which corresponds to the measured data points. After some trials, we decided to fit two polynomials, as shown in fig. 6.7. The result is the following function:

– in case of $0 < E < 8.5 \cdot 10^-2$:

$$S(E) = 0.63817 - 4.2297 \cdot E + 20.96371 \cdot E^2$$

– in case of $8.5 \cdot 10^{-2} < E < 0.4$:

$$S(E) = 0.47968 - 0.81093 \cdot E + 2.85216 \cdot E^2$$

To determine the size of the interesting interval of the energy, the Maxwell distributions for 523K and 700K are shown in fig. 6.8.

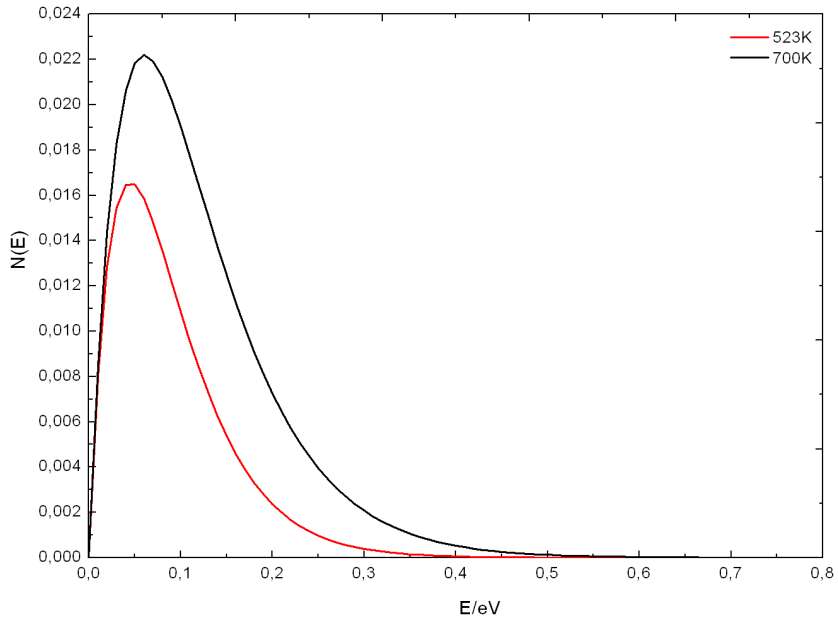

Figure 6.8: The red line shows the Maxwell distribution for a beam at 500K, the black line shows the Maxwell distribution at 700K. The integrals in (6.3) should at least be evaluated until $E = 0.4$ eV.

Using 6.3, the angular distribution of the sticking coefficient can be calculated. The integrals have been evaluated for energies in the range of $E_1 = 0$ until $E_2 = 0.45$. This interval was chosen because the Maxwell distribution at E_2 is almost zero and the fitted function in fig. 6.7 is still plausible. To get the angular distribution of the desorbing particles $D(\vartheta)$, the sticking coefficient $S(\vartheta)$ has to be multiplied by $cos\vartheta$:

$$D(\vartheta) = S(\vartheta) \cdot cos\vartheta \tag{6.4}$$

To calculate 6.3 for different temperatures, we employed a test program which is shown in the appendix. The program calculates the desorption flux according to the fit functions for the respective temperature.

The outputs of the programs are two polar plots: one for the angular distribution of the desorbing particles at 523 K, and one for the angular distribution of the desorbing particles at 700K. In addition, the desorption flux is plotted versus the angle in cartesian coordinates as well, whereby the discrepancy between the angular distribution at the different temperatures can easier be noticed. The polar plots are shown in fig. 6.9 and fig. 6.10. The cartesian plots are shown in fig. 6.11.

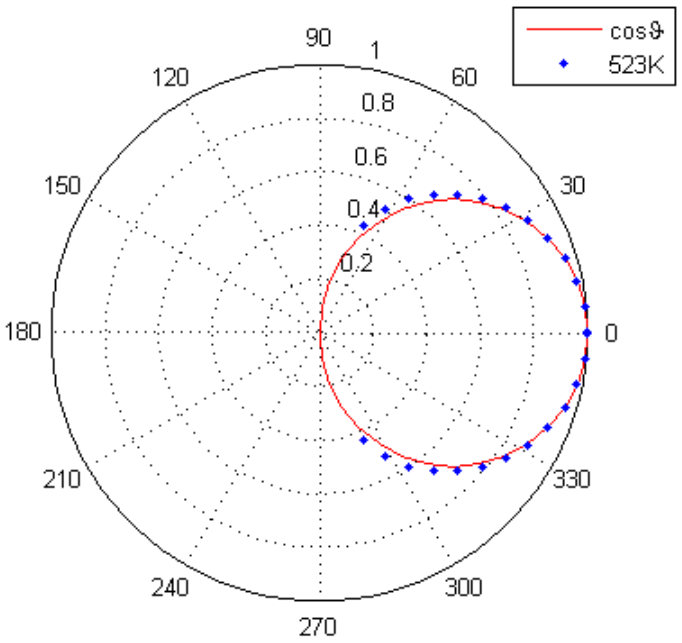

Figure 6.9: The blue dots show the angular distribution at 523K derived from the measured sticking coefficient. The red line is the cosine function.

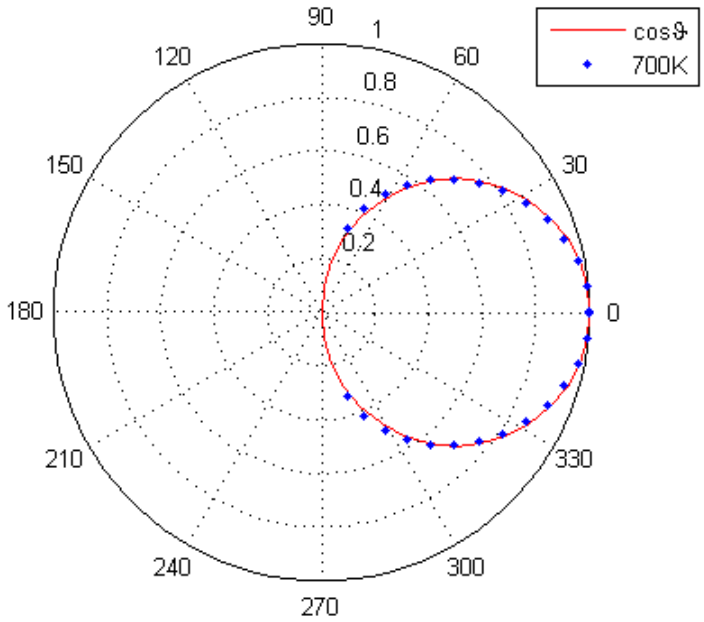

Figure 6.10: The blue dots show the angular distribution at 700K, derived from the measured sticking coefficient. The red line is the cosine function.

There seems to be a small but noticeable discrepancy between the angular distribution at 523K and the angular distribution at 700K. Nevertheless, the resulting angular distribution at 700K is definitely not in the form of $cos^2\vartheta$. The initial declining component of the sticking coefficient seems to annihilate the afterwards slightly increasing part.

Of course, there are many inaccuracies both in measurement and in interpretation, which may cause errors, so that the distributions are not specifiable anymore:

- First of all, as the sticking coefficient has not been measured on the same palladium(111) sample, surface defects on the different samples may cause an error. In addition, we assume the sticking coefficient to be independent of the sample surface temperature. It was not possible to find out at which surface temperature the energy dependance of the sticking coefficient was measured (see [1]).

- The fitted function might not characterize the exact curve progression. Particularly at high energies, the progression of the curve can merely be hypothesized, since there are no more data points. On the other side, the integrals in (6.3) become more accurate at higher energies.

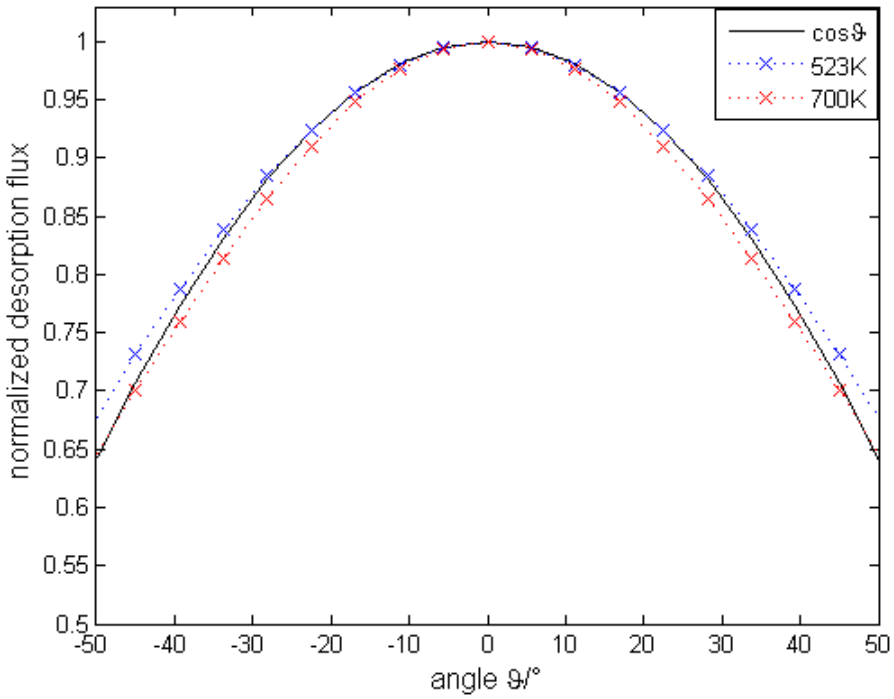

Figure 6.11: The normalized desorption flux is plotted versus the angle. The blue crosses show the angular distribution at 523K, the red crosses show the angular distribution at 700K. These data are derived from the energy dependance of the sticking coefficient measured in [1]. For comparison, the pure $cos\vartheta$ is plotted as well. One can notice that the data at 700K exhibit a sharper angular distribution than the data at 523K.

– Moreover, normal energy scaling has been assumed to be valid. This is usually a reasonable assumption, but in [18] has been shown that for the sticking coefficient of hydrogen on Pd(111), normal energy scaling is not valid anymore at low energies.

The experimental inaccuracies have been mentioned already before. But finally, we can assume that there is not much distinction between the measurements at 523K and 700K, as the sticking coefficient seems to be quite constant in the most important interval, that is the interval where the Maxwell distributions have their maxima. In addition, the measured trend of deuterium desorbing from clean palladium to exhibit sharper angular distribution at higher temperature could be approved.

Chapter 7

Water formation on clean Pd(111) and on Pd(111) + 0.3 MLE VO_x: Measurement results

The water formation on palladium has been investigated for different sample preparations. The results for the respective measurements are shown and the issues are discussed.

7.1 Permeation measurements on Pd(111) and Pd(111) + 0.3 MLE VO_x

The measurement procedure and the measurement difficulties have already been described in chap 4. In this section, the resulting data are analyzed.

In the first instance, fig. 7.1 is considered: The D_2O - signal is plotted versus the oxygen pressure. This measurement was performed on clean palladium at 523K. The more the oxygen pressure increases, the more water is produced. At a certain oxygen pressure, saturation is reached depending on the used deuterium flux: The D_2O - signal does not increase anymore with higher oxygen pressure. The water reaction proceeds very fast on clean palladium, already at low oxygen pressures all deuterium is used to generate water. In addition, the measured D_2O - signal in case of Pd(111) + 0.3 MLE VO_x at 523K is shown in fig. 7.2. In case of Pd(111) + 0.3 MLE VO_x the reaction seems not to saturate as quick as in case of clean palladium. This is quite an interesting feature: the reaction seems to proceed slower when vanadium oxide is on the surface (see fig. 7.2). The absolute amount of produced D_2O should not be compared for these two measurements, as the deuterium flux was not the same.

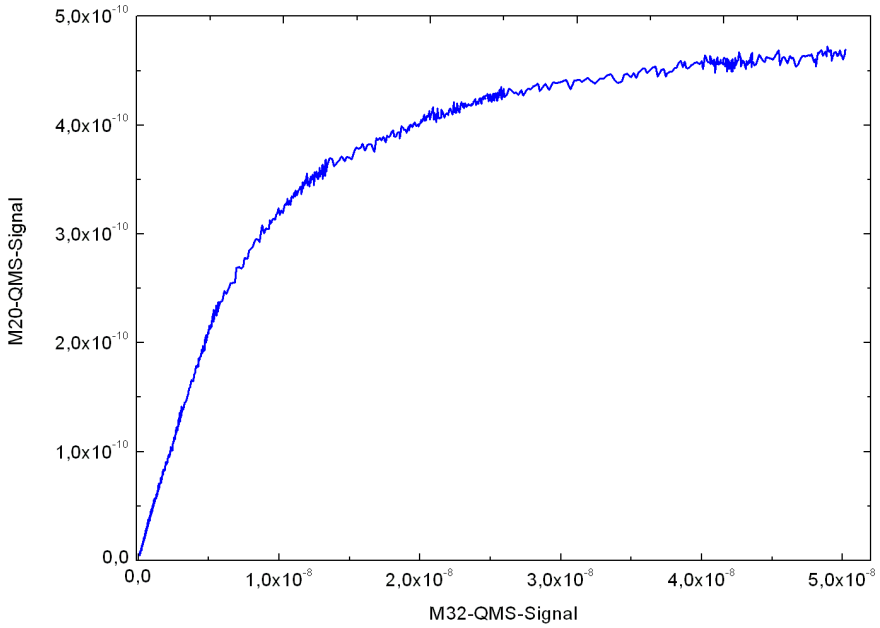

Figure 7.1: Water generation on clean Pd(111) at 523K. The D_2O - signal is plotted versus the O_2 - signal.

7.2 Comparison and discussion of the different permeation measurements

In this section, the different measurement results are compared in terms of the ability to produce water.

The catalytic effect was investigated for four different sample preparations:

- clean Pd(111) at 523K
- clean Pd(111) at 700K
- Pd(111)+0.3 MLE VO_x at 523K
- Pd(111)+0.3 MLE VO_x at 700K

In fig 7.3, the decrease of the deuterium signal is plotted versus the oxygen pressure. All four situations are considered. The deuterium signals instead of the D_2O signals are considered, as they can easily be normalized.

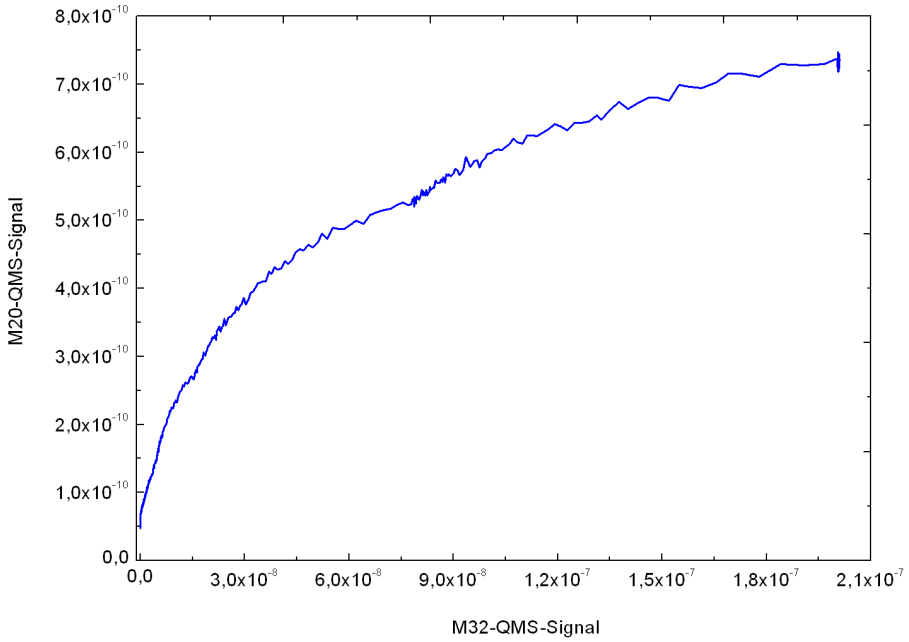

Figure 7.2: Water generation on Pd(111)+0.3MLE VO_x at 523K. The D_2O - signal is plotted versus the O_2 - signal.

– Pd(111)clean

  Obviously, most water is produced on the clean palladium surface at 523 K. Increasing the temperature seems not to influence the amount of produced D_2O, as still all deuterium is used to produce water. But it seems that the reaction happens more slowly at 700K.

– Pd(111)+0.3 MLE VO_x

  Apparently, on the vanadium-covered palladium surface, the reaction proceeds more slowly. Again, a temperature dependance can be noticed.
  At 700 K, all deuterium is used to produce water at sufficient oxygen pressure. In contrast, at 523K, less D_2O is generated: It seems that nearly half of the D_2 desorbs from the surface without reacting with the oxygen.

There can be different reasons for the fact that on Pd(111) + 0.3 MLE VO_x at 523K only half of the deuterium is used to produce water:
One plausible explanation is that the oxygen does not adsorb on the vanadium covered

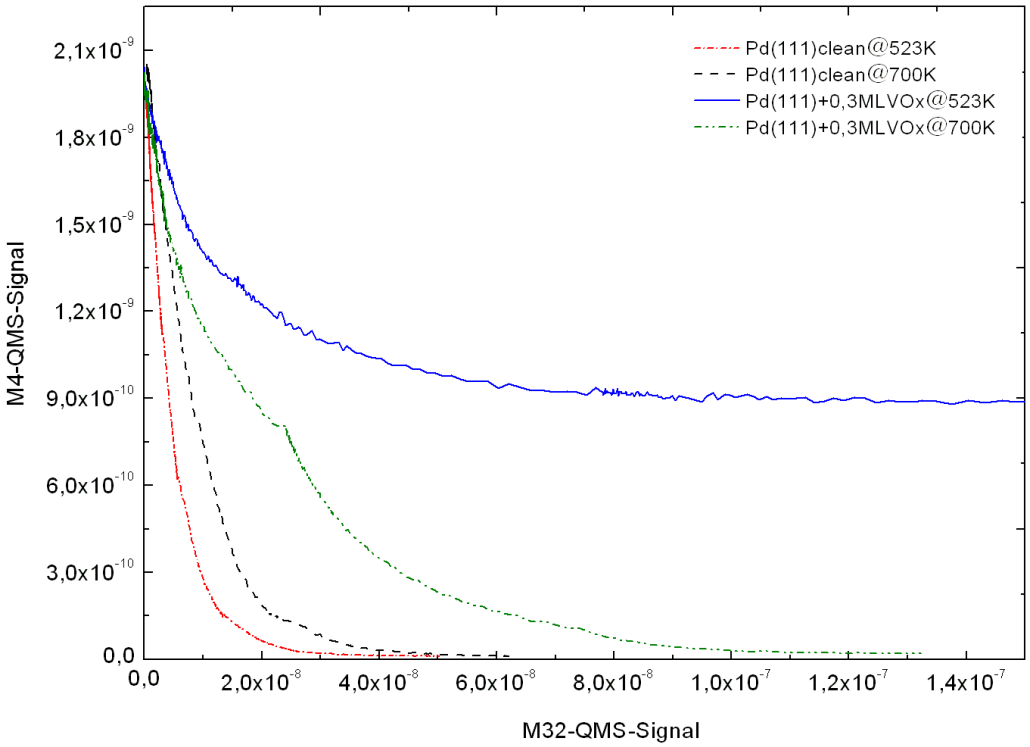

Figure 7.3: The D_2 signal is plotted versus the O_2 - signal. The deuterium decrease for the four different sample preparations is compared. Most water is produced on the clean palladium surface at 523 K. On Pd(111) + 0.3 MLE VO_x at 523K only half of the deuterium is used to produce water.

palladium surface. On this vanadium oxide islands, permeated D_2 desorbs without finding an oxygen atom to react with.

Several physical quantities of importance can be determined by the measurement results:
The slope at the beginning of the D_2O - O_2 function serves as standard for the reaction rate of D_2O, which corresponds to the initial sticking coefficient of oxygen.
These calculations are quite complicate, as many unknown parameters have to be taken into account. Therefor, we pass on quantitative analysis in this thesis. For further information about the sticking coefficient of oxygen on Pd(111) see e.g.[31].

Chapter 8

Conclusion and Summary

In this thesis, we investigated the desorption behavior of deuterium from clean Pd(111) and modified palladium surfaces. The main task of this thesis was the determination of the angular distribution of deuterium desorbing from clean palladium, vanadiumoxide covered and potassium covered palladium. A special feature of this work is that deuterium was supplied to the surface by permeation through the bulk. The advantage of this technique is to establish a continuous desorption flux which allows to analyze desorption parameters with high accuracies. In addition one can also realize various chemical reactions with impinging gas molecules, e.g. the water reaction. To prepare the individual modified surfaces, Pd(111) + 0.3 MLE VO_x and Pd(111) + 0.2 ML K, we used an e-beam evaporator and a getter source, respectively. The coverage of the overlayers was determined by a quartz microbalance. Different surface sensitive methods were employed to examine the palladium surface. The composition of the surface was determined using *Auger electron spectroscopy*. In addition, *low energy electron diffraction* was used to investigate the structure of the surface. The partial pressure was measured by a *quadrupole mass spectrometer*. A second quadrupole mass spectrometer installed in a differentially pumped chamber served as a flux detector which was used for the angular distribution measurements. The distribution was measured by shifting the sample in front of the QMS. In general, angular distributions of desorbing particles are assumed to have the form $cos^n\vartheta$. As the angular distribution was not measured by a directional detector but simply by lateral shift of the sample, Monte Carlo simulations were performed to determine the value of n. Extensive simulations for a number of different experimental situations were performed with the Monte Carlo technique.

The main results concerning the angular distributions for deuterium are the following:

- **Clean Pd(111):**
  At a surface temperature of 523K, the distribution is close to a cosine function, whereas at 700K, the distribution can be best approximated by $cos^2\vartheta$ - function. These results are in good agreement with previous results on deuterium adsorption

by assuming the applicability of detailed balancing.

- **Pd(111) + 0.3 MLE VO_x:**
  At the vanadiumoxide covered palladium surface the angular distribution is slightly sharper than on the clean surface, but the difference is within the experimental error. It should be noted that during the experiment the vanadiumoxide coverage was not reduced.

- **Pd(111) + 0.2 ML potassium:**
  The potassium coverage leads to a further change of the desorption behavior of deuterium. At 523K, the angular distribution can be best approximated by $cos^3\vartheta$ - function. This can be explained by the build up of a higher activation barrier for adsorption. This is again consistent with previous experiments using monoenergetic molecular beams.

The second topic of this work was to investigate the catalytic effect of palladium on the water generation. This was accomplished by dosing molecular oxygen on the differently modified surfaces where deuterium was permeating.

- **Clean Pd(111):**
  On the clean surface all the permeated deuterium could be oxidized to water at a sufficient oxygen partial pressure. The initial change of the water reaction rate as a function of oxygen pressure is determined by the sticking coefficient of oxygen. Since this value is temperature dependant, also the water reaction rate is temperature dependant.

- **Pd(111) +0.3 MLE VO_x:**
  Generally, the water formation rate on the vanadiumoxide covered palladium surface is smaller than on the clean surface. Interestingly, at 523K not all permeating deuterium could be converted into D_2O by impinging oxygen, even not at high oxygen partial pressures. This surprising result will be subject of future investigations.

Appendix A

Calculation of the desorption flux using the fit function S(E)

The program which is used to calculate the desorption flux according to the fitted functions for the respective temperature is shown (see chap.6.2).

```
program to compare the angular distribution with
the measured sticking coefficient
clear all
close all

T=523;
index=0;

Schlange_D=zeros(size(0));

for theta=-32*pi/32:pi/32:32*pi/32
    index=index+1;
    int1=quadl(@(E)func1test(E,theta,T),0,0.085);
    int2=quadl(@(E)func2test(E,theta,T),0.085,0.4);
    int3=quadl(@(E)func3test(E,theta,T),0,0.4);

    Schlange(index)=(int1+int2)/int3;


    Schlange_D(index)=Schlange(index)*cos(theta);
    Vergleich_cos(index)=(cos(theta));

end

thetavec=[-32*pi/32:pi/32:32*pi/32];
```

```
thetavec_grad=[-32*pi/32:pi/32:32*pi/32]/pi*180;

%normize

norm_fac_ind=find(thetavec==0);
norm_fac=Schlange_D(norm_fac_ind);
Schlange_D=Schlange_D./norm_fac;

Schlange_D_grad=Schlange_D/pi*180;
norm_fac_grad=Schlange_D_grad(norm_fac_ind);
Schlange_D_grad=Schlange_D_grad./norm_fac_grad;


Vergleich_cos_grad=Vergleich_cos/pi*180;
Vergleich_cos_grad=Vergleich_cos_grad./(Vergleich_cos_grad(norm_fac_ind));


%make the plot

plot(thetavec_grad,Vergleich_cos_grad,'r');

axis([-80 80 0.3 1]);


xlabel('angle/','Fontsize',12);

ylabel('normalized desorption flux','Fontsize',12);

hold on

plot(thetavec_grad,Schlange_D_grad,'x'); hold off

figure polar(thetavec,Vergleich_cos,'r') hold on
polar(thetavec,Schlange_D,'x') hold off
```

The followinbg functions have been used:

```
function f = func1test(E,theta,T)

f=E/(cos(theta).^2).*exp((-E/cos(theta)^2)./(8.617*10^(-5)*T)).*...
...(0.62025-3.0532.*E+15.37229.*E.^2);
```

```
function f=func2test(E,theta,T)

f=E/(cos(theta).^2).*exp(-(E/(cos(theta)^2))./(8.617*10^(-5)*T)).*...
...(0.47968-0.093.*E+2.85216.*E.^2);

function f =func3test(E,theta,T);

f=E/(cos(theta).^2).*exp(-(E/(cos(theta))^2)./(8.617*10^(-5)*T));
```

Appendix B

The simulation program code

In this section, the program code is presented. Starting the program calls the main page, where one can choose between three geometric configurations: variable distance between emitter and detector, translational displacement of the emitter and tilting the emitter.
Three different programs are necessary depending on the chosen geometry. As the program code is quite long due to the graphical user interface, we show the whole program code merely for the case of varying distance. A quite large part of this program code serves to generate the graphical user interface. We do not show the program code for displacing the emitter, as it is quite similar to the code for varying distance. We present the most important part of the program code for tiling the emitter, which is more interesting. Several functions were used to make the program more clearly. These functions will be explained in the end.
Choosing 'Variable distance' calls the following program:

```
function varargout = gui_Abstand_all(varargin)

% Begin initialization code - DO NOT EDIT
gui_Singleton = 1; gui_State = struct('gui_Name',
mfilename, ...
                   'gui_Singleton',  gui_Singleton, ...
                   'gui_OpeningFcn', @gui_Abstand_all_OpeningFcn, ...
                   'gui_OutputFcn',  @gui_Abstand_all_OutputFcn, ...
                   'gui_LayoutFcn',  [] , ...
                   'gui_Callback',   []);
if nargin && ischar(varargin{1})
    gui_State.gui_Callback = str2func(varargin{1});
end

if nargout
    [varargout{1:nargout}] = gui_mainfcn(gui_State, varargin{:});
```

```
else
    gui_mainfcn(gui_State, varargin{:});
end
% End initialization code - DO NOT EDIT

% --- Executes just before gui_Abstand_all is made visible.
function gui_Abstand_all_OpeningFcn(hObject, eventdata,
handles, varargin)

handles.r_Pr=0; handles.d_DP_anf=0; handles.d_DP_end=0;
handles.Iges=0; handles.n_anf=0; handles.n_end=0;
handles.r_D=0; handles.Detektor_rechteckig=0;
handles.Detektor_rund=0; handles.Probe_rechteckig=0;
handles.Probe_rund=0; handles.a_Prob=0; handles.b_Prob=0;
handles.a_Det=0; handles.b_Det=0;

% Choose default command line output for gui_Abstand_all
handles.output = hObject;

% Update handles structure
guidata(hObject, handles);

% --- Outputs from this function are returned to the command line.
function varargout = gui_Abstand_all_OutputFcn(hObject,
eventdata, handles)

% Get default command line output from handles structure
varargout{1} = handles.output;

% --- Executes on selection change in Probengeometrie.
function Probengeometrie_Callback(hObject, eventdata, handles)

strg=get(hObject,'String'); valg=get(hObject,'Value');
%Set current data to the selected data set

p1=findobj('Tag','Probenradius_text');
p2=findobj('Tag','Probenradius');
p3=findobj('Tag','Probe_text'); p4=findobj('Tag','a_Prob');
p5=findobj('Tag','b_Prob');
p6=findobj('Tag','Seitenlaengen_text2'); switch strg{valg};

    case 'circular'
        handles.Probe_rund=1;
```

```
        handles.Probe_rechteckig=0;
        set(p1,'Visible','on');
        set(p2,'Visible','on');
        set(p3,'Visible','off');
        set(p4,'Visible','off');
        set(p5,'Visible','off');
        set(p6,'Visible','off');

    case 'rectangular'
        handles.Probe_rechteckig=1;
        handles.Probe_rund=0;
        set(p1,'Visible','off');
        set(p2,'Visible','off');
        set(p3,'Visible','on');
        set(p4,'Visible','on');
        set(p5,'Visible','on');
        set(p6,'Visible','on');

end
%save the handles structure
guidata(hObject,handles)

% --- Executes during object creation, after setting all properties.
function Probengeometrie_CreateFcn(hObject, eventdata,
handles)

if ispc && isequal(get(hObject,'BackgroundColor'),
get(0,'defaultUicontrolBackgroundColor'))
    set(hObject,'BackgroundColor','white');
end

% --- Executes on selection change in Detektorgeometrie.
function Detektorgeometrie_Callback(hObject, eventdata,
handles)

strd=get(hObject,'String'); vald=get(hObject,'Value');

d1=findobj('Tag','Detektorradius_text');
d2=findobj('Tag','Detektorradius');
d3=findobj('Tag','Detektor_text'); d4=findobj('Tag','a_Det');
d5=findobj('Tag','b_Det');
d6=findobj('Tag','Seitenlaengen_text'); switch strd{vald};
```

```
    case 'circular'
        handles.Detektor_rund=1;
        handles.Detektor_rechteckig=0;
        set(d1,'Visible','on');
        set(d2,'Visible','on');
        set(d3,'Visible','off');
        set(d4,'Visible','off');
        set(d5,'Visible','off');
        set(d6,'Visible','off');
    case 'rectangular'
        handles.Detektor_rechteckig=1;
        handles.Detektor_rund=0;
        set(d1,'Visible','off');
        set(d2,'Visible','off');
        set(d3,'Visible','on');
        set(d4,'Visible','on');
        set(d5,'Visible','on');
        set(d6,'Visible','on');
end
%save the handles structure
guidata(hObject,handles)

% --- Executes during object creation, after setting all properties.
function Detektorgeometrie_CreateFcn(hObject, eventdata,
handles)

if ispc && isequal(get(hObject,'BackgroundColor'),
get(0,'defaultUicontrolBackgroundColor'))
    set(hObject,'BackgroundColor','white');
end

function a_Prob_Callback(hObject, eventdata, handles)

a_Prob=str2double(get(hObject,'String')); if isnan(a_Prob)
    msgbox('Bitte eine Zahl eingeben','Falsche Eingabe','error');
end handles.a_Prob=a_Prob; guidata(hObject,handles);

% --- Executes during object creation, after setting all properties.
function a_Prob_CreateFcn(hObject, eventdata, handles)

if ispc && isequal(get(hObject,'BackgroundColor'),
get(0,'defaultUicontrolBackgroundColor'))
    set(hObject,'BackgroundColor','white');
```

```
end

function a_Det_Callback(hObject, eventdata, handles)

a_Det=str2double(get(hObject,'String')); if isnan(a_Det)
    msgbox('Bitte eine Zahl eingeben','Falsche Eingabe','error');
end handles.a_Det=a_Det; guidata(hObject,handles);

% --- Executes during object creation, after setting all properties.
function a_Det_CreateFcn(hObject, eventdata, handles)

if ispc && isequal(get(hObject,'BackgroundColor'),
get(0,'defaultUicontrolBackgroundColor'))
    set(hObject,'BackgroundColor','white');
end

function b_Prob_Callback(hObject, eventdata, handles)

b_Prob=str2double(get(hObject,'String')); if isnan(b_Prob)
    msgbox('Bitte eine Zahl eingeben','Falsche Eingabe','error');
end handles.b_Prob=b_Prob; guidata(hObject,handles);

% --- Executes during object creation, after setting all properties.
function b_Prob_CreateFcn(hObject, eventdata, handles)

if ispc && isequal(get(hObject,'BackgroundColor'),
get(0,'defaultUicontrolBackgroundColor'))
    set(hObject,'BackgroundColor','white');
end

function b_Det_Callback(hObject, eventdata, handles)

b_Det=str2double(get(hObject,'String')); if isnan(b_Det)
    msgbox('Bitte eine Zahl eingeben','Falsche Eingabe','error');
end handles.b_Det=b_Det; guidata(hObject,handles);

% --- Executes during object creation, after setting all properties.
function b_Det_CreateFcn(hObject, eventdata, handles)

if ispc && isequal(get(hObject,'BackgroundColor'),
get(0,'defaultUicontrolBackgroundColor'))
    set(hObject,'BackgroundColor','white');
end
```

```
function Probenradius_Callback(hObject, eventdata, handles)

r_Prob=str2double(get(hObject,'String')); if isnan(r_Prob)
    msgbox('Bitte eine Zahl eingeben','Falsche Eingabe','error');
end handles.r_Pr=r_Prob; guidata(hObject,handles);

% --- Executes during object creation, after setting all properties.
function Probenradius_CreateFcn(hObject, eventdata, handles)

if ispc && isequal(get(hObject,'BackgroundColor'),
get(0,'defaultUicontrolBackgroundColor'))
    set(hObject,'BackgroundColor','white');
end

function Abst_anf_Callback(hObject, eventdata, handles)

d_DP_anf=str2double(get(hObject,'String')); if isnan(d_DP_anf)
    msgbox('Bitte eine Zahl eingeben','Falsche Eingabe','error');
end handles.d_DP_anf=d_DP_anf; guidata(hObject,handles);

% --- Executes during object creation, after setting all properties.
function Abst_anf_CreateFcn(hObject, eventdata, handles)

if ispc && isequal(get(hObject,'BackgroundColor'),
get(0,'defaultUicontrolBackgroundColor'))
    set(hObject,'BackgroundColor','white');
end

function abstand_end_Callback(hObject, eventdata, handles)

d_DP_end=str2double(get(hObject,'String')); if isnan(d_DP_end)
    msgbox('Bitte eine Zahl eingeben','Falsche Eingabe','error');
end handles.d_DP_end=d_DP_end; guidata(hObject,handles);

% --- Executes during object creation, after setting all properties.
function abstand_end_CreateFcn(hObject, eventdata, handles)

if ispc && isequal(get(hObject,'BackgroundColor'),
get(0,'defaultUicontrolBackgroundColor'))
    set(hObject,'BackgroundColor','white');
end
```

```
% --- Executes on selection change in popupmenu1.
function popupmenu1_Callback(hObject, eventdata, handles)

str=get(hObject,'String'); val=get(hObject,'Value');

%Set current data to the selected data set
switch str{val};
    case '1000'
        handles.Iges=1000;
    case '10000'
        handles.Iges=10000;
    case '100000'
        handles.Iges=100000;
    case '500000'
        handles.Iges=500000;
    case '1000000'
        handles.Iges=1000000;
end
%save the handles structure
guidata(hObject,handles)

% --- Executes during object creation, after setting all properties.
function popupmenu1_CreateFcn(hObject, eventdata, handles)

if ispc && isequal(get(hObject,'BackgroundColor'),
get(0,'defaultUicontrolBackgroundColor'))
    set(hObject,'BackgroundColor','white');
end

function Detektorradius_Callback(hObject, eventdata, handles)

r_D=str2double(get(hObject,'String')); if isnan(r_D)
    msgbox('Bitte eine Zahl eingeben','Falsche Eingabe','error');
end handles.r_D=r_D; guidata(hObject,handles);

% --- Executes during object creation, after setting all properties.
function Detektorradius_CreateFcn(hObject, eventdata, handles)

if ispc && isequal(get(hObject,'BackgroundColor'),
get(0,'defaultUicontrolBackgroundColor'))
    set(hObject,'BackgroundColor','white');
end
```

```
function Ordnung_anf_Callback(hObject, eventdata, handles)

n_anf=str2double(get(hObject,'String')); if isnan(n_anf)
    msgbox('Bitte eine Zahl eingeben','Falsche Eingabe','error');
end handles.n_anf=n_anf; guidata(hObject,handles);

% --- Executes during object creation, after setting all properties.
function Ordnung_anf_CreateFcn(hObject, eventdata, handles)

if ispc && isequal(get(hObject,'BackgroundColor'),
get(0,'defaultUicontrolBackgroundColor'))
    set(hObject,'BackgroundColor','white');
end

function Ordnung_end_Callback(hObject, eventdata, handles)

n_end=str2double(get(hObject,'String')); if isnan(n_end)
    msgbox('Bitte eine Zahl eingeben','Falsche Eingabe','error');
end handles.n_end=n_end; guidata(hObject,handles);

% --- Executes during object creation, after setting all properties.
function Ordnung_end_CreateFcn(hObject, eventdata, handles)

if ispc && isequal(get(hObject,'BackgroundColor'),
get(0,'defaultUicontrolBackgroundColor'))
    set(hObject,'BackgroundColor','white');
end

% --- Executes on button press in START.
function START_Callback(hObject, eventdata, handles)
%--------------------------------------------------------------------------

%++++++++++++++++++++++ main part of the program++++++++++++++++++++++++++

% --- Definition of the parameters

plot(0,0) drawnow
I0=0;                                   %number of detected particles
Idet=zeros(size(0));                    %fraction of detected intensity
Iges_end=handles.Iges;                  %number of total emitting particles

r_Pr=handles.r_Pr;                      %radius of the emitter
r_D=handles.r_D;                        %radius of the detector
```

```
a_Prob=handles.a_Prob;                  %side length a of the emitter
b_Prob=handles.b_Prob;                  %side length b of the emitter
a_Det=handles.a_Det;                    %side length a of the detector
b_Det=handles.b_Det;                    %side length b of the detector

nexp=0;                                 %exponent of the cosine distribution
n_anf=handles.n_anf;                    %starting exponent
n_end=handles.n_end;                    %end exponent

d_DP_anf=handles.d_DP_anf;              %start distance between
                                         emitter-detector
d_DP_end=handles.d_DP_end;              %end distance between
                                         emitter-detector

lauf=0;                                 %index - legend (not important;-)

Probe_rund=handles.Probe_rund;          %active when emitter is circular
Probe_rechteckig=handles.Probe_rechteckig;  %active when emitter is
                                             rectangular
Detektor_rund=handles.Detektor_rund;    %active when detector is circular
Detektor_rechteckig=handles.Detektor_rechteckig;   %active when detector is
                                                    rectangular

x_m=0;                                  %x-coordinate of the
                                         center point of the detector
y_m=0;                                  %y-coordinate of the
                                         center point of the detector
z_m=0;                                  %z-coordinate of the
                                         center point of the detector

sw=1000;                                %increment to get the
                                         initial point on the emitter
% ----------------------

if Probe_rund
    [x,y,maske,l]=rundeprobe(r_Pr,sw);  %get the initial point
                                         on a circular emitter
elseif Probe_rechteckig                 %get the initial point
                                         on a rectangular emitter
    [x,y,maske,l]=rechteckprobe(a_Prob,b_Prob,sw);
end
```

```
counter=0;                                %counter for the distance
zaehler=0;                                %counter for the exponent
                                           of the cosine distribution n_exp

for nexp=n_anf:n_end                      %loop for the exponent n_exp

    zaehler=zaehler+1;
    counter=0;

    for d_DP=d_DP_anf:d_DP_end           %loop over distance between
                                           emitter and detector

        I0=0;                             %number of detected particles
                                           has to be set at 0
        counter=counter+1;

        for Iges=1:Iges_end               %loop over emitted particles

% --- Generation of a random initial point

        [x_prob, y_prob]=ausgangspunkt(x,y,maske,l);

% --- Generation of the angles theta and phi

        [phi,theta]=winkelgeneration(nexp);

        a=d_DP/cos(theta);        %real distance between the
                                     start-coordinates and the
                                  %target coordinates of the particle

% --- Calculation of the coordinates of the target point

            tra_x=a*sin(theta)*cos(phi);
            tra_y=a*sin(theta)*sin(phi);

            x_det=tra_x+x_prob;
            y_det=tra_y+y_prob;
            z_det=0;
% --- Calculation of the distance to the target point

             if Detektor_rund

                I0=runderDetektor(r_D,x_det,y_det,z_det,x_m,y_m,z_m,I0);
```

```
            elseif Detektor_rechteckig

      I0=rechteckDetektor(a_Det,b_Det,x_det,y_det,z_det,x_m,y_m,z_m,I0);

            end

        end                          %exit the loop over emitted particles

        Idet(counter)=I0/Iges;


    end                               %exit the loop over distance d_DP

Ausgabe(:,zaehler)=Idet; norm_fac=Idet(1);
Ausgabe_norm(:,zaehler)=Ausgabe(:,zaehler)./norm_fac;

end                                   %exit the loop for the exponent n_exp

% --- Graphical display and saving

Daten=[[d_DP_anf:d_DP_end]',Ausgabe];
Daten_norm=[[d_DP_anf:d_DP_end]',Ausgabe_norm];

save dist Daten -ASCII -Tabs  %saves the data in the file 'Abstand_daten'
save dist_norm Daten_norm -ASCII -Tabs
plot([d_DP_anf:d_DP_end],Ausgabe,'LineWidth',1.5)
xlabel('Abstand zwischen Emitter und Detektor in
mm','FontSize',12) ylabel('Intensittsverhltnis
I0/Iges','FontSize',12)

hold on

lauf=1; nn=[n_anf:n_end]; lh=['n=',num2str(nn(1))];

for l=(n_anf+1):n_end                 %to get the legend
    lauf=lauf+1;
    lh=[lh;['n=',num2str(nn(lauf))]];

end legend(lh);

hold off
```

```
% --- Executes on button press in ENDE.
function ENDE_Callback(hObject, eventdata, handles)

close

% --- Executes on button press in Info.
function Info_Callback(hObject, eventdata, handles)
 msgbox('The data are saved as dist.dat and dist_norm.dat','Info','help');
```

Choosing the button 'Tilting' calls the following program (only the interesting main part is shown):

```
function Start_Callback(hObject, eventdata, handles)

warning off plot(0,0); drawnow
% --- Definition of the parameters

I0=0;                                %number of detected particles
Idet=zeros(size(0));                 %fraction of detected intensity
Iges_end=handles.Iges;               %number of total emitting particles

r_Pr=handles.r_Pr;                   %radius of the emitter
r_D=handles.r_D;                     %radius of the detector
d_DP=handles.d_DP;                   %distance between

a_Prob=handles.a_Prob;               %side length a of the emitter
b_Prob=handles.b_Prob;               %side length b of the emitter
a_Det=handles.a_Det;                 %side length a of the detector
b_Det=handles.b_Det;                 %side length b of the detector

nexp=0;                              %Exponent of the
                                    cosine distribution
n_anf=handles.n_anf;                 %starting exponent
n_end=handles.n_end;                 %end exponent

alpha_anf=0;                         % rotation angle
alpha_sw=handles.alpha_sw;           %increment for the rotation
alpha_sw=alpha_sw*2*pi/360;
alpha_end=handles.alpha_end;         %final rotation
alpha_end=alpha_end*2*pi/360;
alphavec=[alpha_anf:alpha_sw:alpha_end];
alphavec=alphavec.*360./(2*pi);

Probe_rund=handles.Probe_rund;       %active when emitter is circular
Probe_rechteckig=handles.Probe_rechteckig; %active when emitter is
                                            rectangular
Detektor_rund=handles.Detektor_rund;  %active when detector is circular
Detektor_rechteckig=handles.Detektor_rechteckig; %active when detector is
                                                    rectangular
```

```
x_m=0;                                  %x-coordinate of the
                                         center point of the detector
y_m=0;                                  %y-coordinate of the
                                         center point of the detector
z_m=0;                                  %z-coordinate of the
                                         center point of the detector

sw=1000;

%-----------------

if Probe_rund
    [x,y,maske,l]=rundeprobe(r_Pr,sw);  %get the initial point on a
                                         circular emitter
elseif Probe_rechteckig                 %get the initial point on a
                                         rectangular emitter
    [x,y,maske,l]=rechteckprobe(a_Prob,b_Prob,sw);
end

counter=0;                              %counter for the angle alpha
alpha=0;                                %angle between emitter and detector
zaehler=0;                              %counter for the exponent n_exp
for nexp=n_anf:n_end                    %loop over n_exp

    zaehler=zaehler+1
    counter=0;

    for alpha=alpha_anf:alpha_sw:alpha_end    %loop over alpha

        I0=0;                           %number of detected particles
                                         is set at 0
        counter=counter+1;
        % - often used angular function
        s_a=sin(alpha);
        c_a=cos(alpha);
        x_m=d_DP*s_a;
        y_m=0;
        z_m=d_DP*c_a;

        for Iges=1:Iges_end           %loop over desorbed particles

% --- Generation of a random initial point
```

```
        [x_prob, y_prob]=ausgangspunkt(x,y,maske,l);

% --- Generation of the angles theta and phi

            [phi,theta]=winkelgeneration(nexp);

            % - simplifications
            s_t=sin(theta);
            c_t=cos(theta);
            s_p=sin(phi);
            c_p=cos(phi);

            %real distance between the start coordinates
                    and the target coordinates of the particles
            a=(1-x_prob/(d_DP/s_a))/((s_t*c_p)/(d_DP/s_a)+c_t/(d_DP/c_a));

% --- Calculation of the coordinates of the target point

            tra_x=a*s_t*c_p+x_prob;
            tra_y=a*s_t*s_p+y_prob;
            tra_z=a*c_t;

            if tra_z>0

                % --- Calculation of the distance to the target point

                if Detektor_rund

                   I0=runderDetektor(r_D,tra_x,tra_y,tra_z,x_m,y_m,z_m,I0);
                elseif Detektor_rechteckig

         I0=rechteckDetektor(a_Det,b_Det,tra_x,tra_y,tra_z,x_m,y_m,z_m,I0);
                end

            end

        end                          %exit the loop over emitting particles

        Idet(counter)=I0/Iges;

    end                              %exit the loop over alpha

    Ausgabe(:,zaehler)=Idet;
```

```
    norm_fac=Idet(1);
    Ausgabe_norm(:,zaehler)=Ausgabe(:,zaehler)./norm_fac;
end                                  %exit the loop for the exponent
                                            of the cosine nexp

% --- Graphical display and saving

Daten=[alphavec',Ausgabe];
Daten_norm=[alphavec',Ausgabe_norm];

save rot Daten -ASCII -Tabs  %saves the data
save rot_norm Daten_norm -ASCII -Tabs

plot(alphavec,Ausgabe,'LineWidth',1.5) xlabel('Verkippung des
Emitters in ','FontSize',12) ylabel('Intensittsverhltnis
I0/Iges','FontSize',12)

hold on

lauf=1; nn=[n_anf:n_end]; lh=['n=',num2str(nn(1))]

for l=(n_anf+1):n_end              %to get the legend
    lauf=lauf+1;
    lh=[lh;['n=',num2str(nn(lauf))]];

end legend(lh)

hold off
```

Several functions were used in these programs. The functions 'rechteckprobe.m' and 'rundeprobe.m' generate point indices according to the respective emitter geometry:

```
function
[x_punkt,y_punkt,maske,lang]=rundeprobe(r_probe,unterteilung)
%creates the points on a circular emitter
 start=r_probe/(unterteilung-1);
 lin=linspace(start,r_probe,unterteilung);
 m=meshgrid(lin);
 n=m';
 x_punkt=m(:);
 y_punkt=n(:);
```

```
 maske=find(sqrt(x_punkt.^2+y_punkt.^2)<=r_probe);
 lang=length(maske);

function
[x_punkt,y_punkt,maske,lang]=rechteckprobe(seite_a,seite_b,unterteilung)
%creates the points on a rectangular emitter
seite_a=seite_a/2;
seite_b=seite_b/2;
start_a=seite_a/(unterteilung-1);              %starting point in the center
lin_a=linspace(start_a,seite_a,unterteilung);
m_a=meshgrid(lin_a);                      x=m_a(:);
start_b=seite_b/(unterteilung-1);
lin_b=linspace(start_b,seite_b,unterteilung);
m_b=meshgrid(lin_b);    n=m_b'; y=n(:); x_punkt=x; y_punkt=y;
maske=find(x>0&y>0);  lang=unterteilung^2;
```

The function 'ausgangspunkt.m' creates a random initial point on the detector:

```
 function
[x_ausgang,y_ausgang]=ausgangspunkt(x,y,maske,l)
%generates a random initial point
xy_in=maske(floor(rand*l)+1); xy_ausgang=[x(xy_in),y(xy_in)];
%a quadrant is determined randomly
if rand<0.5
    x_ausgang=-xy_ausgang(1);
else
    x_ausgang=xy_ausgang(1);
end if rand<0.5
    y_ausgang=-xy_ausgang(2);
else
    y_ausgang=xy_ausgang(2);
end
```

The functions 'runderDetektor.m' and 'rechteckDetektor' select detected particles on a circular and on a rectangular detector.

```
function I0=runderDetektor(r_D,x,y,z,x_m,y_m,z_m,I0)
%Selection of detected particles on a circular detector
abstand=sqrt((x-x_m)^2+(y-y_m)^2+(z-z_m)^2);

if abstand<=r_D
      I0=I0+1;
end
```

```
function I0=rechteckDetektor(a,b,x,y,z,x_m,y_m,z_m,I0)
%Selection of detected particles on a rectangular detector
y_abs=sqrt((y-y_m)^2); xz_abs=sqrt((x-x_m)^2+(z-z_m)^2); if
y_abs<=b & xz_abs<=a
    I0=I0+1;
end
```

The function 'winkelgeneration.m' generates the angles ϑ and φ according to the $cos^n\vartheta$ - distribution.

```
function [phi,theta]=winkelgeneration(nexp);
%generates the values for the angles theta and phi
 phi=rand*2*pi;
    if phi==0
        phi=rand*2*pi;
    end
exponent=1/(nexp+1); theta=acos((1-rand)^exponent);
```

Bibliography

[1] M. Riedler, Diploma thesis, TU Graz, (1996).

[2] J.A. Barker and D.J. Auerbach, Surf. Sci. Rep., 4: 1-99, (1985).

[3] J.C. Polanyi and H.G. Wong, J. Chem. Phys. 51, 1439, (1969).

[4] J.E. Lennard-Jones, Trans. Farady. Soc. 28, 333-359, (1932).

[5] R.I. Masel, Wiley Series in Chemical engineering, (1996).

[6] A. Winkler and K.D. Rendulic, Mod. Rev. Phys. Chem. 11(1), 101-133, (1992).

[7] A. Gross, J. Chem. Phys. 102, 5045, (1995).

[8] I. Langmuir, J. Chem. Phys. 54, 376, (1971).

[9] K.D. Rendulic and A. Winkler, Surf. Sci. 299, 261-276, (1994).

[10] W. van Willigen, Phys. Letters A 28, 80, (1968).

[11] G. Comsa and R. David, Surf. Sci. Rep. 5, 145, (1985).

[12] C. Eibl and A. Winkler, J. Chem. Phys. 117(2), 834-841, (2002).

[13] G. Anger, A. Winkler and K.D. Rendulic, Surf. Sci. 220, 1-17, (1989).

[14] F. A. Brockhaus, Spectrum, Brockhaus der Naturwissenschaften, (2003).

[15] G. Pauer, Dissertation, TU Graz, (2005).

[16] M. Kratzer, Diploma thesis, TU Graz, (2005).

[17] M. Prutton, Oxford Physics Series 11, (1975).

[18] C. Resch, H.F. Berger, K.D. Rendulic, E. Bertel, Surf. Sci. 316, 1105-1109, (1994).

[19] C. Klein, G. Kresse, S. Surnev, F. P. Netzer, M. Schmidt and P. Varga, Physic. Rev. B 68, 235416, (2003).

[20] J. Schoiswohl, M. Sock, S. Surnev, M.G. Ramsey, F.P. Netzer, G. Kresse, J.N. Andersen, Surf. Sci. 555, 101-117, (2004).

[21] F.P. Leisenberger, S. Surnev, L. Vitali, M.G. Ramsey, F. P. Netzer, J. Vac. Sci. Technol. A 17(4), 1743 - 1749, (1999).

[22] M. Sambi, S. Surnev, G. Kresse, F.P. Netzer, G. Granozzi, Physic. Rev. B 68, 155417, (2003).

[23] G. Kresse, S. Surnev, J. Schoiswohl, F.P. Netzer, Surf. Sci. 555, 118-134, (2004).

[24] M. Kratzer, S. Surnev, F.P. Netzer and A. Winkler, J. Chem. Phys. 125, 074703, (2006).

[25] A. Winkler and J. T. Yates, J. Vac. Sci. Technol. A 6(5), 2929-2933, (1988).

[26] H. Pölzl, Diploma thesis, TU Graz, (1996).

[27] J. Greenwood, Vacuum 67(2), 217-222, (2002).

[28] Y. Suetsugu, J. Vac. Sci. Technol. A 14(1), 245-250, (1995).

[29] B. Seiwald, Diploma thesis, TU Graz, (1998).

[30] T. Engel and H. Kuipers, Surf. Sci. 90, 162-180, (1979).

[31] P. Sjövall and P. Uvdal, J. Vac. Sci. Technol. A 16(3), 943-947, (1998).